Astron. Astrophys. 273, 451–472 (1993)

ASTRONOMY AND ASTROPHYSICS

Infrared photometry and spectrophotometry of SN 1987A

II. November 1987 to March 1991 observations*

P. Bouchet[1] **and I.J. Danziger**[2]

[1] ESO, Casilla 19001, Santiago 19, Chile
[2] ESO, Karl-Schwarzschild-Str. 2, W-8046 Garching bei Munchen, Germany

Received June 9, accepted November 13, 1992

Abstract. We present the infrared (1–20 μm) observations of SN 1987A obtained at ESO La Silla between 29 October 1987 and 27 March 1991 (day 1493); photometry and narrow band CVF spectrophotometry ($\lambda/\Delta\lambda \approx 60$) were acquired during that period. The infrared light curves and the spectra are shown and discussed. The spectral energy distribution is dominated by an increasing IR excess after day 530 (beyond 3.5 μm) due to the presence of dust in the envelope which was first discovered by its spectroscopic signature. We show that dust is still present at least until day ~1400, and that the two zone model for the expanding envelope, suggested from the visible spectra obtained at ESO, can account for the observed changes in the near-infrared colours in the period days 530–560.

Hydrogen lines, observed in the spectrum from the very beginning, are present until day 1109 (although Brγ is hardly noticeable on the 9 March 1990 spectrum) and we describe the variations of their intensities throughout our monitoring period. Attention is drawn to the presence of CO emission observed until November 1988, and to the evolution of cobalt through the observation of the fine structure line of [Co II] at 10.52 μm. The temporal behaviour of the emission lines due to [Ni I] 3.12 μm and [Si I] + [Fe II] 1.644 μm are also shown.

Key words: infrared radiation – photometry – spectrophotometry – supernovae and supernova remnants: SN 1987A

1. Introduction

The impact of the discovery of SN 1987A on modern astronomy was instantly recognised by the international community of observers. This has led to the accumulation of a large quantity of good quality, frequently spaced data for which the European Southern Observatory (ESO) has dedicated a considerable amount of observing time.

Quite often the data set of observations covering the complete wavelength range accessible at La Silla has been used to elucidate physical conditions and mechanisms obtaining in the SN envelope. For example, (i) the study of dust condensation in the ejecta of the supernova after 500 d – which was first detected at ESO by Danziger et al. (1989) – by Lucy et al. (1989, 1991a); (ii) the elaboration of the bolometric light curve – in collaboration with Cerro Tololo Interamerican Observatory (CTIO) – by Suntzeff & Bouchet (1990; hereafter Paper II), Bouchet et al. (1991a), and Bouchet et al. (1991b; hereafter Paper III) which demonstrate the need for an extra energy source in addition to the radioactive decay of ^{56}Co after day ~900; (iii) the temporal behaviour and abundances of molecules, dust and atomic species in the expanding envelope by Danziger et al. (1991a); (iv) the temporal behaviour of various emission lines by Danziger et al. (1991b, c); (v) the demonstration of non-thermal excitation of line emission by Lucy (1991), and Lucy et al. (1991b). An account of most of these results is given in Bouchet (1990).

We present in this paper the infrared photometric and spectrophotometric data (1–20 μm) upon which these works are partly based. They have accumulated from our monitoring of SN 1987A that was initiated at ESO on 1 March 1987, seven days after outburst. The first results (until October 1987) are published (Bouchet et al. 1987; Bouchet et al. 1989a, hereafter Paper I) and we emphasize here the data obtained since that date until 27 March 1991 (day 1493) (Sect. 2). A detailed report of the whole set of observations until 9 March 1990 is given in Bouchet (1990). We show the infrared light curves of SN 1987A (Sect. 3), and the evolution with time of the spectral energy distribution throughout that period (Sect. 4), which is dominated by excess emission observed longward of 5 μm (Sect. 4.1). Our results are compared in Sect. 5 with the ones of the SAAO group.

We also examine the evolution of the hydrogen, CO, [Co II], [Fe II], [Si I] and [Ni I] emission lines, and briefly

Send offprint requests to: P. Bouchet
* Based on observations obtained at ESO, La Silla

discuss some problems associated with our observations of carbon monoxide and cobalt (Sect. 6).

2. Observations

2.1. Infrared photometry

Broad-band infrared photometry of SN 1987A was made with the standard ESO infrared photometers (Bouchet 1989) attached to the 1, the 2.2 and the 3.6 m telescopes at La Silla (the two latter being provided with an f/35 wobbling secondary mirror). These photometers are equipped with InSb detectors (1–5 μm) and Ga–Ge bolometers (8–20 μm); observing parameters are given in Paper I. The filters and detectors are essentially the same at the three telescopes, and there are no systematic differences in the photometry from one telescope to the other. The effective wavelength and the absolute flux calibration used for each filter, as well as the photometric standards and the procedure used to reduce the observations, are described in Paper I.

The apertures used were 15, 8 and 7.5″ at the 1, 2.2 and 3.6 m telescopes respectively. After August 1989, the 1 m telescope was not used, and the InSb measurements were made with the 2.2 and the 3.6 m telescopes, while all the Bolometer measurements (10 and 20 μm) were made exclusively at the 3.6 m telescope. Beginning January 1990, the diaphragm size was 5″ at the 3.6 m telescope. After December 1990, SN 1987A was too faint to be observed through the $N1$ ($\lambda_0 = 8.36$ μm; $\Delta\lambda = 0.85$ μm FWHM), $N2$ ($\lambda_0 = 9.67$ μm; $\Delta\lambda = 1.65$ μm FWHM), and $N3$ ($\lambda_0 = 12.89$ μm; $\Delta\lambda = 3.7$ μm FWHM) filters and we used the wider N filter ($\lambda_0 = 10.36$ μm; $\Delta\lambda = 5.2$ μm FWHM) instead.

A frame obtained in 12 November 1989, with the ESO imaging InfraRed Array Camera, IRAC (experimental at that time) with the 2.2 m telescope at La Silla showed that the companion star No. 2 (West et al. 1987) had magnitudes about 14.7 in J and H, and about 14.8 in K, and thus contaminates our photometry by 0.01 mag in these filters on day 640 (23 November 1988). In the absence of more accurate photometry, we correct our results in J, H, and K according to these approximate values, and assume that $L = 14.8$ for this star. The corresponding correction amounts to 0.5 and 0.1 mag by 9 March 1990, and to 0.75 and 0.2 mag by 27 March 1991 for K and L, respectively. No correction for the contribution of stars 3 and 4 has been applied to the tabulated data.

The journal of observations and the photometric results are given in Tables 1–3. The light curves obtained through the J to Q_0 filters are shown in Figs. 1 and 2, and the evolution with time of the colours $(J-H)$, $(H-K)$, $(K-L)$, and $(K-M)$ are displayed in Fig. 3. We have included in these figures the data presented in Paper I. Note that these data have not been corrected for interstellar extinction.

The discrepancy reported between ESO and CTIO results at 10 and 20 μm has been discussed in Paper III

Table 1. 1–5 μm photometry

MJD[a]	t[b]	J (±)	H (±)	K (±)	L (±)	M (±)
47097.45	248.13	3.69	3.78	3.26	2.27	0.68
		0.02	0.02	0.02	0.03	0.04
47101.48	252.16	3.72	3.81	3.30	2.33	0.73
47103.47	254.15	3.73	3.83	3.29	2.34	0.71
47103.48	254.16	3.74	3.84	3.33	2.34	0.72
47105.36	256.04	3.78	3.89	3.37	2.38	0.77
47105.37	256.05	3.78	3.88	3.35	2.36	0.73
47105.38	256.06	3.79	3.90	3.37	2.37	0.75
47106.40	257.08	3.77	3.90	3.38	2.38	0.77
47106.41	257.09	3.79	3.91	3.39	2.39	0.76
47107.44	258.12	3.79	3.91	3.40	2.39	0.76
47107.45	258.13	3.80	3.92	3.40	2.39	0.76
47107.46	258.14	3.80	3.93	3.42	2.40	0.78
47108.37	259.05	3.80	3.93	3.42	2.41	0.77
47108.38	259.06	3.79	3.93	3.42	2.42	0.77
47125.05	275.73	4.03	4.17	3.70	2.65	0.93
47125.06	275.74	4.04	4.17	3.71	2.67	0.92
47125.31	275.99	4.04	4.17	3.71	2.66	0.92
47138.16	288.84	4.13	4.28	3.86	2.77	1.08
47138.17	288.85	4.15	4.29	3.86	2.78	1.08
47161.20	311.88	4.42	4.58	4.21	3.02	1.32
47161.31	311.99	4.47	4.66	4.28	3.08	1.30
47163.29	313.97	4.51	4.68	4.31	3.11	1.38
47164.08	314.76	4.52	4.66	4.30	3.11	1.34
47164.09	314.77	4.52	4.66	4.30	3.11	1.33
47168.10	318.78	4.52	4.72	4.37	3.16	1.43
47170.21	320.89	4.60	4.76	4.41	3.18	1.43
47172.16	322.84	4.57	4.75	4.42	3.18	1.39
47173.13	323.81	4.61	4.75	4.43	3.21	1.44
47178.09	328.77	4.68	4.81	4.51	3.28	1.49
47178.10	328.78	4.68	4.81	4.52	3.27	1.50
47197.08	347.76	4.97	5.06	4.83	3.52	1.76
47197.09	347.77	4.97	5.06	4.83	3.52	1.78
47198.17	348.85	4.93	5.04	4.82	3.52	1.73
47198.18	348.86	4.92	5.03	4.81	3.50	1.70
47199.06	349.74	4.95	5.04	4.85	3.53	1.76
47199.07	349.75	4.95	5.05	4.85	3.53	1.76
47199.08	349.76	4.95	5.05	4.84	3.53	1.75
47199.94	350.62	4.95	5.08	4.87	3.53	1.75
47199.95	350.63	4.95	5.07	4.87	3.53	1.76
47203.20	353.88	4.98	5.08	4.89	3.57	1.78
47203.21	353.89	4.97	5.07	4.88	3.57	1.77
47203.22	353.90	4.98	5.07	4.88	3.57	1.76
47211.10	361.78	5.09	5.18	5.01	3.66	1.79
47211.11	361.79	5.09	5.18	5.01	3.67	1.79
47221.04	371.72	5.21	5.31	5.20	3.80	2.01
47221.05	371.73	5.23	5.31	5.21	3.80	2.01
		0.02	0.02	0.02	0.03	0.04
47229.09	379.77	5.32	5.38	5.30	3.85	2.05
47230.01	380.69	5.33	5.40	5.32	3.88	2.06
47230.02	380.70	5.32	5.40	5.31	3.88	2.01
47231.02	381.70	5.32	5.39	5.32	3.86	2.09
47231.03	381.71	5.35	5.40	5.33	3.86	2.06
47247.01	397.69	5.54	5.56	5.57	4.09	2.28
47247.02	397.70	5.55	5.58	5.57	4.12	2.24
47248.01	398.69	5.51	5.53	5.54	4.09	2.24

Table 1 (continued)

MJD[a]	t^b	J (±)	H (±)	K (±)	L (±)	M (±)
47256.86	407.54	5.62	5.66	5.71	4.22	2.30
47256.87	407.55	5.61	5.65	5.71	4.22	2.33
47258.91	409.59	5.65	5.69	5.73	4.28	2.31
47258.92	409.60	5.62	5.66	5.72	4.26	2.29
47259.87	410.55	5.68	5.71	5.76	4.30	2.36
47259.88	410.56	5.69	5.70	5.76	4.29	2.34
47270.85	421.53	5.84	5.81	5.92	4.37	2.45
47272.85	423.53	5.83	5.83	5.94	4.42	2.48
47272.86	423.54	5.85	5.84	5.96	4.42	2.45
47274.83	425.51	5.87	5.85	5.96	4.45	2.54
47274.84	425.52	5.88	5.84	5.97	4.40	2.51
47275.83	426.51	5.90	5.87	6.01	4.46	2.53
47275.84	426.52	5.89	5.87	5.99	4.44	2.48
47276.82	427.50	5.88	5.87	6.01	4.45	2.57
47276.83	427.51	5.89	5.89	5.99	4.45	2.56
47288.80	439.48	6.07	5.98	6.19	4.67	2.64
47288.81	439.49	6.09	5.99	6.19	4.66	2.64
47290.93	441.61	6.10	6.02	6.24	4.66	2.64
47292.88	443.56	6.14	6.04	6.27	4.71	2.68
47303.84	454.52	6.28	6.16	6.46	4.86	2.78
		0.03	0.03	0.03	0.03	0.04
47305.69	456.37	6.34	6.17	6.43	4.81	2.78
		0.03	0.03	0.03	0.04	0.05
47305.70	456.38	6.33	6.19	6.44	4.83	2.80
47306.90	457.58	6.30	6.18	6.44	4.79	2.81
47307.79	458.47	6.31	6.20	6.47	4.81	2.79
47307.81	458.49	6.33	6.20	6.46	4.81	2.75
47309.04	459.72	6.33	6.18	6.45	4.80	2.76
47309.05	459.73	6.34	6.19	6.47	4.82	2.82
47311.79	462.47	6.35	6.23	6.48	4.85	2.82
47311.80	462.48	6.37	6.23	6.50	4.84	2.81
47315.76	466.44	6.37	6.24	6.55	4.91	2.85
47315.77	466.45	6.39	6.26	6.56	4.91	2.85
47316.83	467.51	6.38	6.27	6.56	4.93	2.82
47316.84	467.52	6.38	6.26	6.56	4.90	2.81
47338.81	489.49	6.78	6.52	6.89	5.14	3.07
47341.56	492.24	6.75	6.53	6.91	5.14	3.09
47343.47	494.15	6.75	6.53	6.93	5.15	3.08
		0.03	0.03	0.03	0.04	0.05
47343.49	494.17	6.77	6.56	6.96	5.16	3.11
47366.59	517.27	7.13	6.83	7.31	5.40	3.32
		0.04	0.04	0.04	0.04	0.06
47366.60	517.28	7.12	6.82	7.29	5.38	3.31
47367.77	518.45	7.21	6.90	7.35	5.42	3.28
47368.39	519.07	7.20	6.89	7.36	5.43	3.28
47368.40	519.08	7.18	6.88	7.37	5.45	3.29
47376.44	527.12	7.29	6.97	7.48	5.50	3.42
47376.45	527.13	7.29	6.97	7.49	5.50	3.43
47377.44	528.12	7.33	6.99	7.51	5.53	3.47
47378.43	529.11	7.30	7.00	7.52	5.53	3.42
47382.50	533.18	7.44	7.06	7.58	5.55	3.48
47382.51	533.19	7.44	7.07	7.57	5.57	3.49
47383.47	534.15	7.42	7.07	7.59	5.60	3.50
47383.48	534.16	7.44	7.07	7.60	5.55	3.55
47398.39	549.07	7.68	7.29	7.83	5.69	3.68
47398.40	549.08	7.68	7.28	7.82	5.65	3.65
47406.46	557.14	7.87	7.44	7.99	5.76	3.85
47406.47	557.15	7.88	7.44	8.00	5.72	3.81
47431.44	582.12	8.44	7.92	8.48	6.03	4.09
		0.05	0.05	0.05	0.04	0.06
47432.45	583.13	8.44	7.94	8.49	6.15	4.04
47433.44	584.12	8.45	7.94	8.48	6.07	4.08
47434.43	585.11	8.43	8.00	8.54	6.04	4.12
47456.29	606.97	8.93	8.46	9.00	6.45	4.37
		0.05	0.05	0.05	0.05	0.07
47458.34	609.02	8.94	8.47	9.00	6.39	4.31
47460.29	610.97	8.93	8.50	9.05	6.54	4.55
47467.39	618.07	9.09	8.66	9.19	6.67	4.48
47468.33	619.01	9.13	8.69	9.21	6.69	4.58
47484.42	635.10	9.37	8.91	9.47	6.91	4.71
		0.05	0.05	0.05	0.03	0.04
47484.42	635.10	9.37	8.91	9.47	6.91	4.71
		0.05	0.05	0.05	0.05	0.04
47486.36	637.04	9.46	9.01	9.49	—	—
47486.37	637.05	9.44	9.01	9.50	—	—
47487.35	638.03	9.43	9.01	9.52	—	—
47487.36	638.04	9.43	9.01	9.52	—	—
47488.10	638.78	9.41	9.02	9.53	6.95	4.85
		0.04	0.04	0.04	0.11	0.11
47491.13	641.81	9.53	9.12	9.62	7.14	4.86
		0.04	0.04	0.04	0.12	0.11
47491.14	641.82	9.53	9.12	9.62	7.17	4.88
		0.04	0.04	0.04	0.12	0.11
47519.15	669.83	9.93	9.58	10.04	7.61	5.44
		0.04	0.04	0.04	0.08	0.11
47540.05	690.73	10.12	9.77	10.31	8.10	—
		0.04	0.04	0.04	0.32	—
47540.07	690.75	10.14	9.78	10.30	8.23	5.63
		0.04	0.04	0.04	0.25	0.10
47541.16	691.84	10.19	9.82	10.33	8.34	5.83
		0.04	0.04	0.04	0.18	0.12
47542.13	692.81	10.17	9.83	10.35	8.61	5.87
		0.04	0.04	0.04	0.19	0.14
47542.15	692.83	10.17	9.83	10.37	8.59	5.61
		0.04	0.04	0.04	0.20	0.16
47543.13	693.81	10.18	9.83	10.38	8.34	5.77
		0.04	0.04	0.04	0.13	0.15
47544.14	694.82	10.19	9.84	10.37	8.33	5.91
		0.04	0.04	0.04	0.18	0.18
47545.17	695.85	10.16	9.83	10.37	8.59	5.85
		0.04	0.04	0.04	0.21	0.24
47547.11	697.79	10.24	9.90	10.44	8.41	5.84
		0.04	0.04	0.04	0.26	0.17
47571.08	721.76	10.56	10.22	10.74	9.01	6.26
		0.04	0.04	0.04	0.12	0.12
47574.02	724.70	10.57	10.25	10.81	8.83	6.39
		0.04	0.04	0.04	0.12	0.12
47575.04	725.72	10.57	10.28	10.83	8.90	6.42
		0.04	0.04	0.04	0.11	0.07
47580.04	730.72	10.63	10.32	10.87	9.02	6.55
		0.04	0.04	0.04	0.10	0.07
47581.02	731.70	10.63	10.33	10.88	9.02	6.50
		0.04	0.04	0.04	0.07	0.09
47582.11	732.79	10.66	10.34	10.94	9.21	6.60
		0.04	0.04	0.04	0.05	0.07
47582.03	732.71	10.63	10.33	10.90	9.49	6.34
		0.04	0.04	0.04	0.21	0.20

Table 1 (continued)

MJD[a]	t[b]	J (±)	H (±)	K (±)	L (±)	M (±)
47582.06	732.74	10.63	10.32	10.89	9.06	6.77
		0.04	0.04	0.04	0.22	0.10
47587.02	737.40	10.73	10.38	10.97	9.08	6.51
		0.04	0.04	0.04	0.22	0.12
47602.10	752.78	10.81	10.55	11.08	—	—
		0.04	0.04	0.04	—	—
47607.05	757.73	10.93	10.63	11.16	9.26	7.04
		0.04	0.04	0.04	0.58	0.50
47608.04	758.72	10.89	10.60	11.27	9.15	6.79
		0.04	0.04	0.04	0.48	0.33
47615.04	765.72	10.95	10.73	11.29	—	—
		0.04	0.04	0.04	—	—
47635.00	785.68	11.16	10.94	11.52	—	—
		0.04	0.04	0.04	—	—
47641.96	792.64	11.29	11.01	11.60	9.85	7.44
		0.04	0.04	0.04	0.17	0.26
47662.98	813.66	11.47	11.16	11.80	—	—
		0.04	0.04	0.04	—	—
47724.44	875.12	12.13	11.95	12.48	—	—
		0.04	0.04	0.04	—	—
47752.40	903.08	12.36	12.20	12.61	11.21	8.91
		0.04	0.04	0.04	0.28	0.33
47753.41	904.09	12.29	12.17	12.59	10.81	9.23
		0.04	0.04	0.04	0.19	0.34
47841.35	992.03	13.20	13.14	13.32	11.90	9.87
		0.04	0.04	0.04	0.27	0.53
47880.23	1030.91	13.34	13.41	13.40	11.74	—
		0.04	0.04	0.04	0.28	—
47903.20	1053.88	13.59	13.62	13.65	11.99	10.65
		0.07	0.07	0.07	0.28	0.50
47930.13	1080.81	13.77	13.79	13.72	—	—
		0.04	0.04	0.04	—	—
47959.06	1109.74	14.20	14.19	14.11	11.98	10.93
		0.06	0.06	0.06	0.41	0.57
48166.24	1316.92	15.33	15.30	14.78	13.04	—
		0.06	0.06	0.06	0.25	—
47129.22	279.90	0.93	1.15	0.21	−0.85	
		0.02	0.04	0.05	0.32	
47140.11	290.79	0.92	1.16	0.22	−0.53	
		0.02	0.02	0.03	0.09	
47160.24	310.92	0.99	1.39	0.29	−0.51	
		0.02	0.03	0.04	0.12	
47163.15	313.83	1.09	1.43	0.43	−0.42	
		0.03	0.05	0.06	0.15	
47198.11	348.79	1.17	1.62	0.78	—	
		0.10	0.15	0.30	—	
47211.13	361.81	1.25	1.63	0.80	—	
		0.10	0.15	0.25	—	
47229.06	379.74	1.32	1.84	0.96	−0.69	
		0.07	0.21	0.26	0.43	
47247.03	397.71	1.26	—	1.09	—	
		0.10	—	0.36	−0.39	
47247.05	397.73	1.38	1.91	1.06	0.40	
		0.07	0.17	0.18	—	
47249.01	399.69	1.49	1.92	1.06	−0.23	
		0.05	0.07	0.11	0.31	
47250.86	400.54	1.42	1.94	1.05	−0.33	
		0.04	0.05	0.10	0.35	
47305.79	456.47	1.53	2.19	0.90	—	
		0.10	0.21	0.20	—	
47312.76	463.44	1.59	2.03	1.10	—	
		0.03	0.06	0.06	—	
47369.44	520.12	1.71	1.78	1.17	0.14	
		0.04	0.05	0.06	0.12	
47376.45	527.13	1.70	1.71	1.12	0.34	
		0.04	0.05	0.05	0.13	
47464.45	615.13	1.95	1.70	0.91	—	
		0.11	0.15	0.21	—	
47465.24	615.92	1.85	1.71	0.50	—	
		0.08	0.09	0.10	—	
47465.25	615.93	1.82	1.68	0.59	—	
		0.07	0.04	0.11	—	
47485.43	636.11	2.13	1.72	0.74	−0.64	
		0.10	0.09	0.13	0.37	
47485.45	636.13	2.17	1.75	0.76	−0.74	
		0.08	0.09	0.08	0.35	
47489.42	640.10	2.15	1.71	0.80	−0.48	
		0.05	0.05	0.04	0.22	
47489.44	640.12	2.17	1.74	0.84	−0.35	
		0.04	0.05	0.05	0.20	
47490.15	640.83	2.27	1.76	0.79	−0.12	
		0.06	0.07	0.03	0.43	
47519.19	669.87	2.51	2.20	0.89	−0.91	
		0.19	0.13	0.19	0.44	
47541.08	691.76	2.99	2.35	1.40	—	
		0.21	0.15	0.25	—	
47547.15	697.83	3.12	2.60	1.48	−0.12	
		0.20	0.32	0.40	0.50	
47547.18	697.86	3.16	2.52	1.58	−0.20	
		0.19	0.17	0.44	0.46	
47583.12	733.80	3.82	3.01	1.64	—	
		0.22	0.16	0.18	—	
47584.02	734.70	3.54	3.10	1.74	−0.43	
		0.23	0.16	0.20	0.40	
47641.99	792.67	4.65	4.01	2.41	0.73	
		0.25	0.29	0.28	0.29	

[a] Modified Julian date.
[b] Days after outburst; $t_0 = 46849.316$ (February 23.316, 1987; Arnett et al., 1989). When no errors are specified for a measurement, the previous ones apply.

Table 2. 8–20 μm photometry

MJD[a]	t[b]	$N1$ (±)	$N2$ (±)	$N3$ (±)	Q_0 (±)
47112.24	262.92	0.76	0.84	−0.18	−1.22
		0.06	0.09	0.11	0.25
47127.21	277.89	0.85	1.03	0.13	—
		0.09	0.10	0.12	—
47127.23	277.91	0.89	1.15	0.11	−0.98
		0.08	0.09	0.13	0.41

Table 2 (continued)

MJD[a]	t^b	$N1$ (±)	$N2$ (±)	$N3$ (±)	Q_0 (±)
47753.44	904.12	6.42	5.54	3.64	1.31
		0.34	0.11	0.18	0.13
47841.39	992.07	6.59	5.20	—	—
		0.44	0.31	—	—
47842.36	993.04	—	—	3.61	1.34
		—	—	0.27	0.45
47880.23	1030.91	7.25	5.71	4.10	1.27
		0.44	0.45	0.35	0.38
47881.20	1031.88	6.00	5.13	3.26	1.29
		0.47	0.44	0.34	0.30

[a] Modified Julian date.
[b] Days after outburst; $t_0 = 46849.316$ (February 23.316, 1987; Arnett et al., 1989).

Table 3. N and Q_0 photometry

MJD[a]	t^b	N (±)	Q_0 (±)
47880.23	1030.91	5.49	1.27
		0.29	0.38
47881.20	1031.88	6.07	1.29
		0.33	0.30
47903.14	1053.82	6.40	1.52
		0.26	0.33
47904.18	1054.86	6.38	1.74
		0.19	0.20
47930.13	1080.81	6.35	2.40
		0.19	0.25
47959.06	1109.74	6.20	2.56
		0.31	0.20
48166.36	1317.04	7.43	3.46
		0.46	0.54
48342.05	1492.73	7.65	—
		0.48	—

[a] Modified Julian date.
[b] Days after outburst; $t_0 = 46849.316$ (February 23.316, 1987; Arnett et al., 1989).

Table 4. Journal of the CVFs observations

Date	CVF1	CVF2	CVF3	CVF4
1987 28/02	+	+	+	−
03/03	+	+	+	−
05/03	+	−	−	−
15/03	+	−	−	+
21/03	+	+	−	−
29/03	+	+	−	−
31/03	+	+	−	−
02/04	+	+	−	−
06/04	+	+	−	−
10/04	+	−	−	−
12/04	−	+	−	−
22/04	−	−	−	+
01/05	+	−	−	−
09/05	+	+	−	−
14/05	−	+	−	−
05/06	+	+	+	+
08/06	+	+	+	+
10/06	+	+	−	+
15/06	+	−	−	+
17/06	−	+	−	−
19/06	−	+	−	−
21/06	+	−	−	−
24/06	+	+	−	−
31/07	−	+	−	−
02/08	−	+	+	−
04/09	−	+	+	−
09/09	+	−	−	−
12/09	−	−	−	+
04/11	+	−	−	−
06/11	−	−	+	−
08/11	+	−	−	−
12/11	−	−	−	+
27/11	−	−	−	+
03/12	−	+	+	−
08/12	+	+	+	−
30/12	−	−	−	+
1988 02/01	−	−	−	+
17/01	+	+	+	−
07/02	+	−	−	−
29/02	+	−	−	−
10/03	+	−	−	−
27/03	−	+	−	−
30/03	−	−	−	+
06/04	−	−	−	+
08/04	+	+	+	−
21/04	−	+	−	−
24/04	+	−	−	−
09/05	+	−	−	−
25/05	−	−	+	−
31/05	−	−	−	+
03/06	−	+	−	−
28/06	−	+	+	−
23/07	+	+	−	−
25/07	+	−	−	−
01/08	+	+	−	−
08/08	+	+	+	−
24/08	+	+	−	−
27/09	+	−	−	−
29/09	−	+	+	−
22/10	+	−	−	−
25/10	+	−	−	−
18/11	−	+	−	−
21/11	−	−	−	+
24/11	−	−	−	+
1989 13/01	+	−	−	−
17/01	+	−	−	−

Table 4 (continued)

Date	CVF1	CVF2	CVF3	CVF4
16/02	+	−	−	−
25/02	−	−	−	+
29/03	+	−	−	−
20/12	+	−	−	−
1990 08/02	+	−	−	−
01/03	+	−	−	−
04/03	+	+	−	−
07/03	+	−	−	−
20/03	+	+	−	−
28/03	+	+	−	−
30/03	+	+	−	−
01/04	+	−	−	−
05/04	+	−	−	−
09/04	−	+	−	−
11/04	−	+	−	−
13/04	−	+	−	+
23/04	+	+	+	−
08/05	+	+	+	+
13/05	+	−	+	−
15/05	+	+	+	−
07/06	+	+	+	+
09/06	+	+	−	+
13/06	−	+	−	+
16/06	+	+	−	+
18/06	+	−	+	−
20/06	+	+	−	−
23/06	+	+	−	−
30/07	+	−	+	−
01/08	+	−	−	−
05/08	−	+	−	−
05/09	+	−	−	−
11/09	−	−	−	+
05/10	−	+	+	−
05/11	−	+	+	−
07/11	−	+	−	−
09/11	+	−	+	−
25/11	+	+	+	−
29/11	−	−	−	+
04/12	+	−	−	−
10/12	−	−	−	+
31/12	+	+	−	−
03/01	+	+	+	−
05/02	−	−	+	−
08/02	−	+	−	−
09/03	−	+	+	−
26/03	+	−	−	−
28/03	−	−	+	+
02/04	−	−	−	+
07/04	+	−	−	−
19/04	+	−	−	−
23/04	+	+	−	−
07/05	−	+	+	−
23/05	+	+	−	−
30/05	−	+	+	−
01/06	−	−	−	+
04/06	+	−	−	−
30/06	+	+	+	−
24/07	−	−	+	+
26/07	−	+	−	+
03/08	+	−	−	+
09/08	+	+	+	−
01/09	−	+	−	−
28/09	−	+	+	−
21/10	−	+	+	−
23/10	−	+	−	−
02/11	+	−	−	−
20/11	−	−	−	+
22/11	+	−	−	−
23/12	+	−	−	−
15/01	+	−	−	−
18/01	+	−	−	−
17/02	−	+	+	−
26/02	−	−	−	+
15/08	+	−	−	−
11/01	+	−	−	−
09/03	+	−	−	−

Notes: CVF1: 1.5–2.4 μm; CVF2: 2.8–4.2 μm; CVF3: 4.6–5.4 μm; CVF4: 8–13 μm.

and by Suntzeff et al. (1991, 1992). Its consequence for the evaluation of the flux distribution in the far infrared, and thus for the calculation of the bolometric luminosity has also been elaborated. This discrepency between the two sets of data is still not explained.

2.2. *Spectrophotometry*

Spectrophotometry at a resolving power of ($\lambda/\Delta\lambda \sim 60$) has been obtained in the 1–5 μm range using three different CVFs (circular variable filters) and an InSb detector, and in the 8–14 μm range using one CVF and a Ga–Ge bolometer. Information concerning the standard stars and the reduction procedure are given in Paper I. The journal of the spectrophotometric observations is given in Table 4. Selected spectra are presented in Figs. 5–7a, b. A complete set of CVF data is available in Bouchet (1990) and some in the 10 μm range are presented in Bouchet et al. (1991c). These figures display the spectral evolution of the supernova in the different wavelength ranges. They show that there is still flux in the continuum, at least until the epoch of our last CVF observations (day 1110; see also Bouchet 1990). There are also strong emission lines present in all parts of the spectra, the most conspicuous of which are those with large widths due to velocity broadening in the expanding envelope where they originate. Figure 8 shows the overall spectrum taken on 23–24 July 1988 and the identifications of the main features. A detailed description of the spectra can be found in Oliva et al. (1987, 1989) and Meikle et al. (1989).

We discuss and present measurements of the main emission lines in Sect. 6. Of particular importance is the observation in our spectra (until August, 1988; see Fig. 7a)

of the longer wavelength half (>8 μm) of the broad feature ascribed to a molecular band of silicon monoxide (SiO) by Rank et al. (1988). Our analysis of this band in detail is restricted because of the atmospheric cut-off shortward of 8 μm (Danziger et al. 1991a).

3. The light curves

The *J*, *H*, *K* and *L* light curves (Fig. 1) are by now well known, and have been discussed in several papers. These light curves have been described in Paper I until day 250: at this point the envelope had became optically thin, and the decline in each band was linear, consistent with the luminosity being produced by the decay of $\sim 0.07 M_\odot$ of ^{56}Co. Although these light curves display quite similar trends, they have different slopes which is due in part to the varying contribution of emission lines (in particular Brγ and CO 2.3 μm in the *K* band, CO 4.6 μm in the *M* band, and [Si I] + [Fe II] 1.644 μm in the *H* band; we will show (Sect. 6.2) that, between day 300 and 530, the intensity of this last line decreases far more slowly than the intensity of the nearby continuum, which probably explains the slower decrease of the *H* light curve with respect to *J* and *K* during that period). This linear decline continues until day ~530, when its rate increases markedly: this has been interpreted as the photometric evidence of dust formation (Lucy et al. 1989, 1991a; Paper II; Danziger et al. 1991a–c). This steeper decline then slows down, first at day ~650 in all the light curves, and then quite markedly in the *K* and *L* bands at day ~760; this latter change coincides with a change in the profile of [O I] 6300 Å and other emission lines, and is accompanied by a less rapid decrease of their luminosities. This change at day 760 has been interpreted in terms of a simplified 2 zone model by Danziger et al. (1991b, c): if the envelope consists of a higher velocity hotter region and a lower velocity cooler region which was cooling faster, then around day 650 the luminosity of this lower velocity material might have dropped so that the higher velocity material started to become more evident. The preceding authors (and also Spyromilio et al. 1991) suggest that this could possibly mark the onset of the IR catastrophe. The domination of the hotter component as evidenced by the behaviour of the width of [O I] 6300 (Danziger et al. 1991b) would be complete by day ~800. It is striking that the flattening of the bolometric light curve occurs at this epoch (Bouchet et

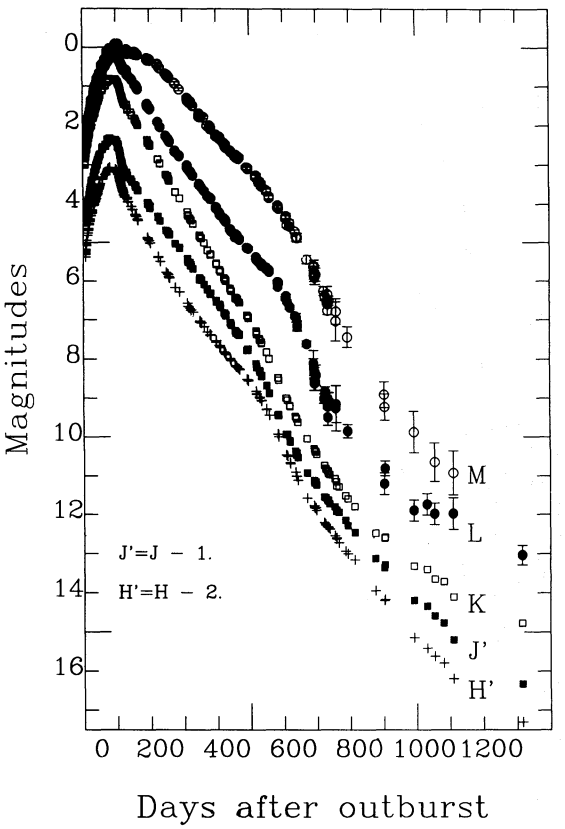

Fig. 1. ESO *J*, *H*, *K*, *L*, *M* broad band photometry between days 13 and 1316

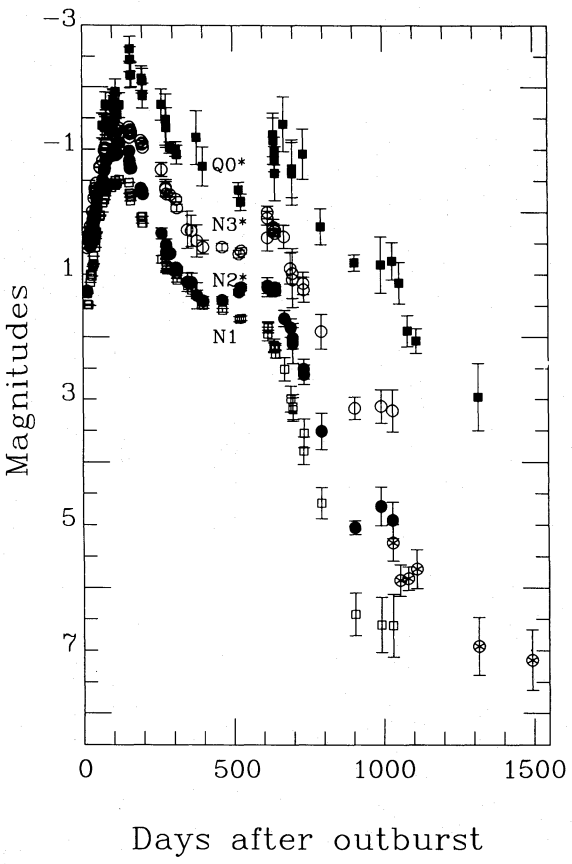

Fig. 2. ESO *N*, *N*1, *N*2, *N*3, and Q_0 broad band photometry between days 13 and 1316. The *N*, *N*2, *N*3, and Q_0 data have been shifted for clarity (the plotted values are $N^* = N - 0.5$; $N2^* = N2 - 0.5$; $N3^* = N3 - 0.5$; $Q_0^* = Q_0 - 0.5$). The filled circles correspond to *N*2, while the crossed ones correspond to *N*

al. 1989b; Paper III; Suntzeff et al. 1991, 1992). The decrease of the light curves slows down again after day ~1100.

The M light curve shows the same general behaviour as the K and L ones, although it is dominated by the presence of carbon monoxide (CO) until the dust formation.

The changes in the colours (Fig. 3) are related to the emission spectrum and the cooling of the dust component (Paper III). For instance, the $(K-M)$ light curve monitors the changing strength of CO until dust formation. Between day 400 and 600, the luminosity of the CO 2.3 μm line (in the K band) decreases by a factor ~38, while the luminosity of the CO 4.6 μm line (in the M band) decreases by a factor ~8 (Danziger et al. 1991a; Bouchet 1990). The only other prominent line affecting these two bands is Brγ which is located in the K band; during the same period, this line has faded by a factor ~26. Therefore, if the flux through these bands were due only to the emission lines, one would expect a reddening of the $(K-M)$ index of ~0.7 mag. The continuum is also reddened by 0.3 mag after dust has formed (Paper III), which is consistent with the observed value of $\Delta(K-M)$ ~1 mag. The same simple analysis can be done with the $(K-L)$ colour: in contrast with the SAAO results (see Sect. 5), the ESO L filter is not affected by the [Ni I] 3.12 μm line, but rather by Brα which decreases by a factor of ~19 during the period considered. The $(J-K)$ and $(H-K)$ colours are not affected by the cooling of the dust component and monitor only the respective evolution of the emission lines. Of special interest is the $(H-K)$ colour because the [Si I] + [Fe II] 1.644 μm line lies in the H band: the decrease of the intensity of this line is slower than that of Brγ and CO 2.3 μm, which explains the blueing of the $(H-K)$ colour after day ~200. The onset of dust formation (day 530) marks a stronger fading of the 1.644 μm (Lucy et al. 1991a), and then reverses the trend of $(H-K)$ as can be seen in Fig. 3.

It is noteworthy that the colours displayed in Fig. 3 all show a dramatic turn-down in their evolution at day ~650, while no special trend is apparent in the bolometric light curve and no obvious changes are detected in the optical line luminosities at this epoch. However, we have already noted that the decrease of luminosity is slowed down in all the bands at this date. The fact that all the near-IR colours were so strongly affected (i.e. became suddenly bluer) can be explained by a distinctive slowing in the rate of dust condensation at that time and the

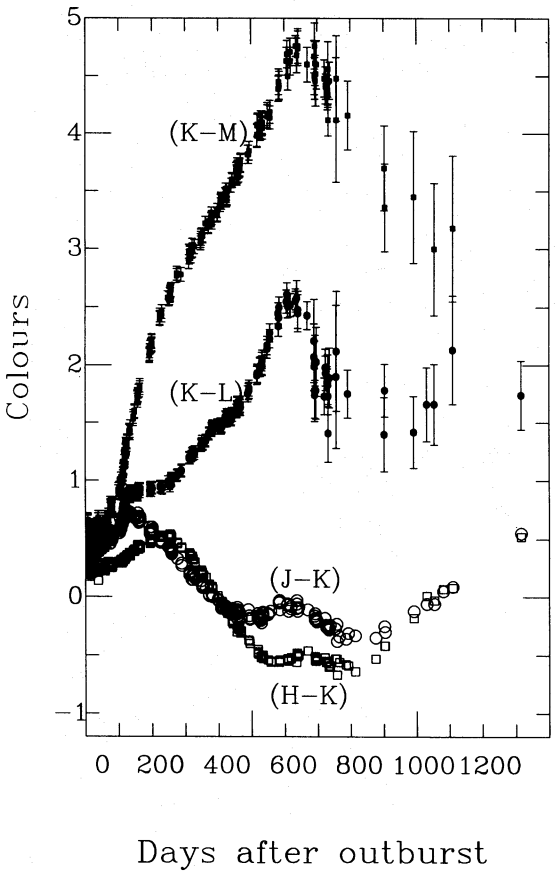

Fig. 3. Near-infrared colours $(J-K)$, $(H-K)$, $(K-L)$ and $(K-M)$ between days 13 and 1316

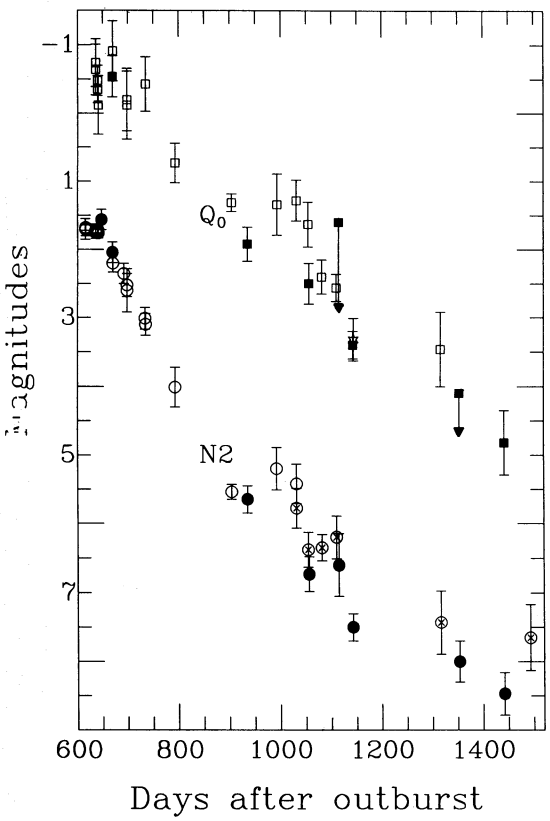

Fig. 4. ESO and CTIO 10 and 20 μm broad band photometry between days 600 and 1316. The open points are from ESO: circles correspond to $N2$ (until day 1030) and crossed circles to N (from day 1054); the filled points are from CTIO, where only N has been measured

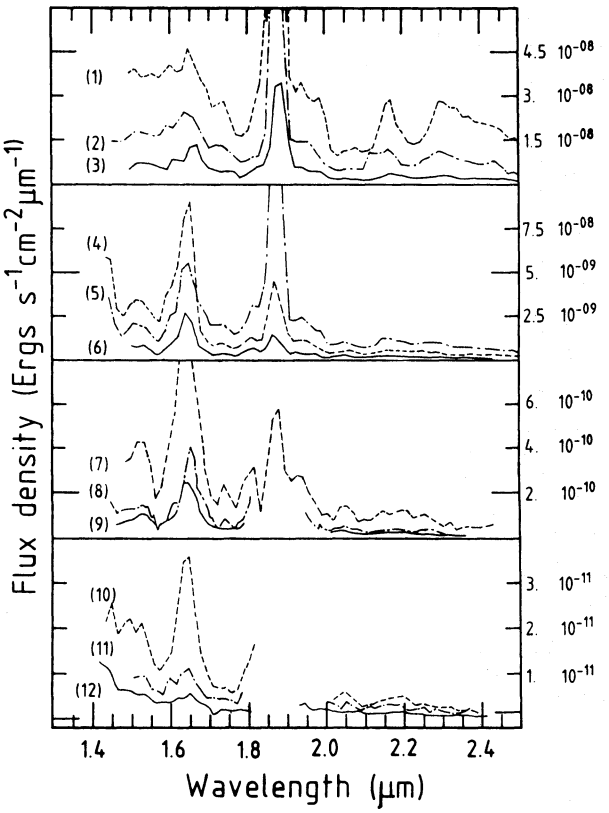

Fig. 5. CVF spectra in the 1.4–2.4 μm region for the following dates: (1) 04/11/87; (2) 31/12/87; (3) 26/03/88; (4) 04/06/88; (5) 23/07/88; (6) 27/09/88; (7) 02/11/88; (8) 17/01/89; (9) 16/02/89; (10) 15/08/89; (11) 20/12/89; (12) 09/03/90

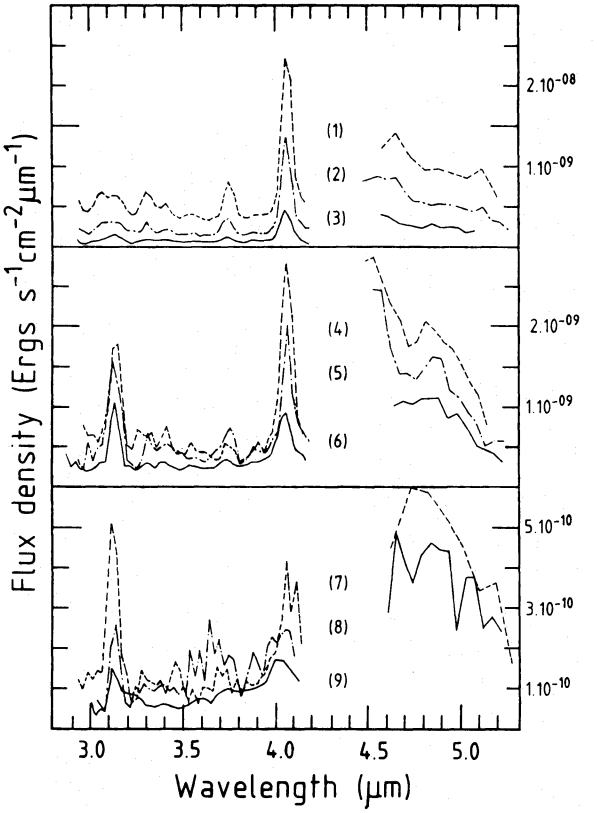

Fig. 6. CVF spectra in the 2.9–5.4 μm region for the following dates: (1) 05/11/87; (2) 03/01/88; (3) 27/03/88; (4) 07/05/88; (5) 30/05/88; (6) 23/07/88; (7) 29/09/88; (8) 21/10/88; (9) 18/11/88

formation of clumps: at that point, the temperature of the dust component is nearly stabilized (i.e. not much reddening of the spectrum due to decrease of temperature), and the bulk of it is in opaque clouds which geometrically occult the background emission. It must therefore be the average background emission that became bluer during that period. This may be due to the emergence of the hotter material in the higher velocity zone (see above). At day ~800, the process has been completed and the blueing stops. The changes in the near-IR colours are well correlated with the observed changes in the profiles and the luminosities of emission lines.

The 10 and 20 μm light curves, being strongly influenced by the thermalization of the hard radiation by the dust, show a somewhat different trend: the luminosity decreases until day ~400, then increases to maximum at day ~650, and decreases again until day ~900. After some levelling until day ~1050, it resumes its decrease. Although the scatter in the data points in Fig. 2 is large, there is indication that the decrease is slowed down after day ~1200. Of special interest is the $N2$ light curve: at the onset of dust formation it displays an increase more pronounced than in the other light curves. As this effect is less obvious in the $N1$ filter, it cannot be attributed to a continuous reddening of the supernova. Since the $N2$ filter is centered by design on the peak of the silicate emission band, the behaviour of the light curve in this filter may be interpreted as enhanced emission from diffuse silicate dust before it becomes completely optically thick. This effect relative to that of the neighbouring photometric bands would be reduced later when black body radiation from the clumped dust became dominant (Bouchet et al. 1991c).

Although dust formation has been detected by spectroscopic means (i.e. an apparent blueward shift of several emission lines; Danziger et al. 1989), it has been confirmed by an independent analysis of the infrared light curves (Lucy et al. 1989; Paper II; Paper III). If we apply the same photometric criteria, the light curves presented here clearly show no indication of disappearance of the dust at least until day ~1400. This confirms the observations made by Danziger et al. (1991b, c) that the criterion of line shift reveals that dust is still present up until that epoch.

4. The spectral energy distribution

Figures 9a–d show the spectral energy distribution at selected dates derived from our photometry and our CVFs

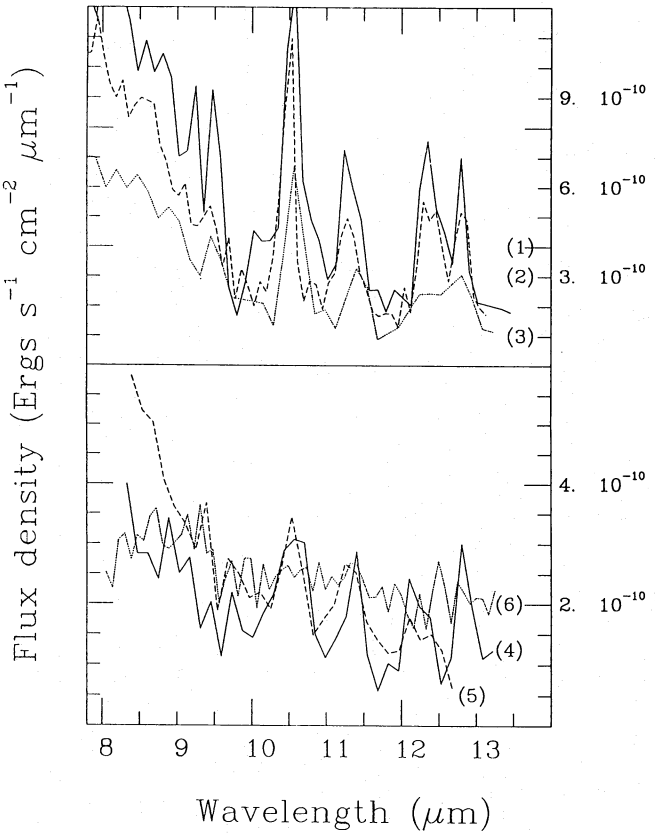

Fig. 7a. CVF spectra in the 8–13 μm region for the following dates: (1) 12/11/87; (2) 30/12/87; (3) 02/04/88; (4) 01/06/88; (5) 03/08/88; (6) 21/11/88

measurements. They illustrate how the photospheric spectrum after the explosion gradually evolves towards a nebular one (although some continuum is still present in all the figures), with a cool thermal component longward of 5 μm developing after August 1988. The identifications of the main features present in the 1–20 μm range are given in Fig. 8. Note the strength of the fundamental vibration band of CO at 4.6 μm visible until October 1988 (day 610) which contributes significant flux to the *M* band, and of the first overtone band at 2.3 μm. These figures (Figs. 9a–d) show also the development of the [Ni I] emission line at 3.12 μm, which became stronger than Brα by July 1988.

We note that the presence of a cooler component in the spectral energy distribution of SN 1987A appeared clearly less than one month after the explosion (Paper I). As is shown in Paper II and Paper III, by day 635 it affected the fluxes from *L* to Q_0 and accounts for ~50% of the total UV–Optical–IR flux of the supernova. Yet, Paper II shows that it seems to have continuously evolved in time, and thus could be attributed to an early and continual formation of dust, starting around day 100. It is not possible, however, to rule out that multiple effects have conspired to produce the uniform variation. In Paper II, it was argued that the infrared excess from day 20 to day 300 (at the time that a cool clearly dustlike component appears) could be due to the evolution of a dense optically thick plasma radiating like a blackbody to a low-density optically thin plasma radiating by free–free emission. It was also argued in Paper I that the early observed excess emission in the near-IR could be due to free–free emission. The presence of free–free emission superimposed upon the thermal dust emission is discussed in Paper III and Wooden (1990), who invoked (up until day 415) thermal emission from dust in a very close CS shell.

Regardless of the cause of this early infrared excess, and the fact that it may have increased continuously, the most striking point in Fig. 9b is the rapid change in the flux distribution longward of 8 μm between August and October 1988. Part of evidence for the presence of dust in the envelope consists in this increasing IR excess which eventually dominated the radiative output of SN 1987A (Bouchet et al. 1991c). This has been discussed in detail elsewhere (Paper II; Paper III), but here we note that the original analysis of the bolometric light curve was consistent with the dust thermalizing the harder radiation generated by the radioactive β-decay of ^{56}Co and emitting as a blackbody at the temperature imposed by the dilute radiation field. Again, our last observations clearly show that the thermal dust emission is still the major component of the spectral energy distribution.

If one uses only the IR data near 10 and 20 μm, both broad band photometry and CVF scans, there is evidence that an IR excess began to grow earlier than day 530, the suggested time of dust formation from optical spectra. Inspection of Fig. 2 and measurement of the flux in the CVF scans in Fig. 7b suggests that the IR flux began to show an excess as early as day 460.

5. Comparison with the SAAO work

The observations reported here parallel and complement the comparably-sampled infrared photometric observations of the SAAO group covering the *JHKL* bands until day 792 (Menzies et al. 1987; Catchpole et al. 1987, 1988, 1989; Whitelock et al. 1988, 1989). We have compared our photometric observations in the *J*, *H*, *K* and *L* bands with the similar data from SAAO. Bersanelli et al. (1991) at ESO, and Glass (1985) and Carter (1990) at SAAO, point out that although the filters used for *JHKL* photometry are intended to match the clear bands of atmospheric transmission, exact matching of the filters or even precise replication of existing ones is extremely difficult. Also, differences in the atmospheric transmission from one site to the other may affect the effective wavelengths and the cut-off of the bands. It is clear then, that for an object with an unsmooth spectrum such as SN 1987A one might expect differences between the two sets of photometric data. The transmission curves for the ESO and SAAO filters are given in Paper I. Both *K* filters compare well, while the

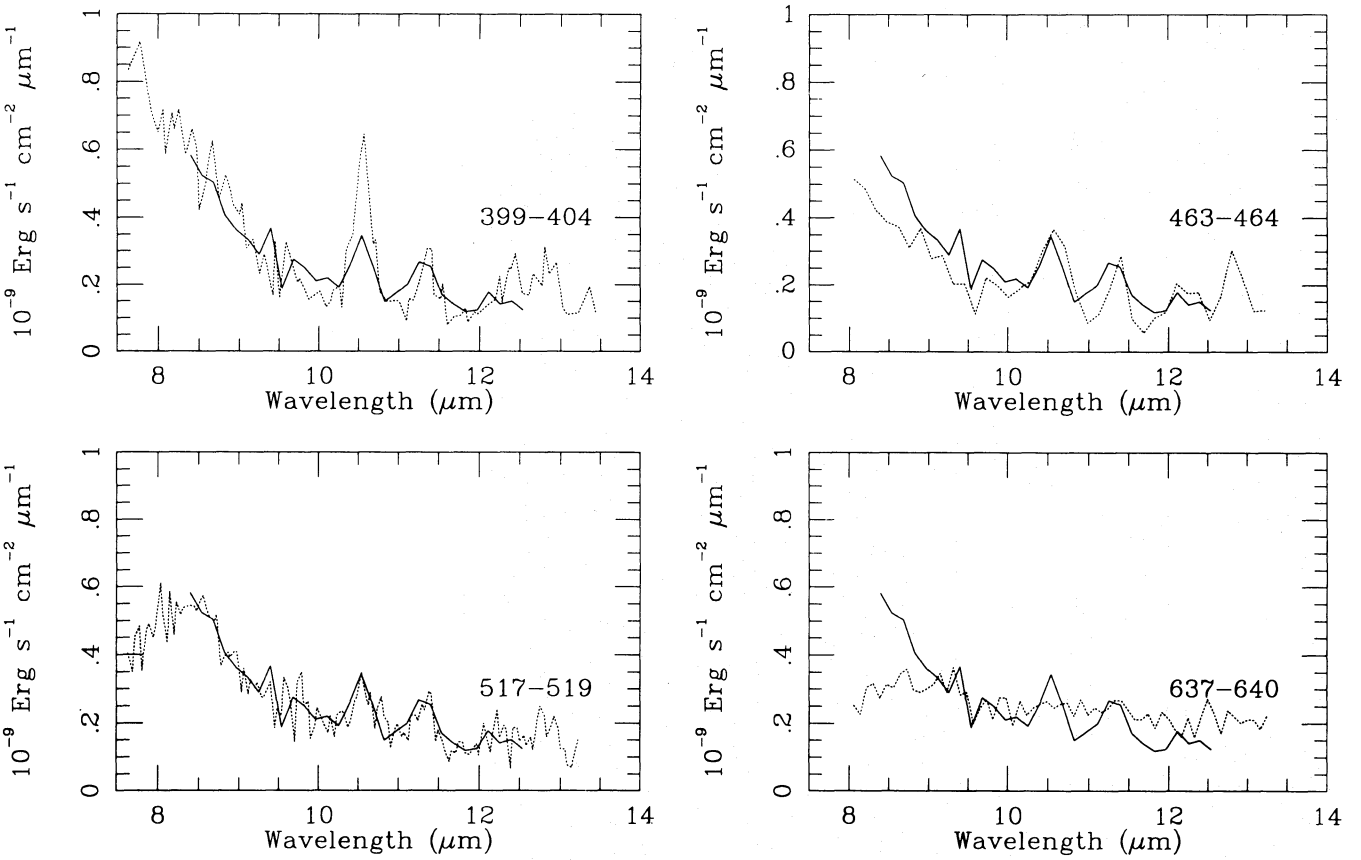

Fig. 7b. Evolution of the CVF spectra in the 8–13 μm region between day 399 (28 March 1988) and 640 (24 November 1988); each averaged spectrum (for the indicated dates) is represented by a dotted line and is compared with the spectrum obtained on 3 August 1988 (day 527). Note that no change is apparent in the continuum between day 399 and day 527, which seems to rule out the possibility that dust might have condensed before that date

effective wavelengths of the ESO J and H filters are significantly redder than the SAAO ones. ESO uses (as do many other groups) an L filter centered at 3.78 μm (sometimes called L'). The use of this filter avoids the problem caused by the atmospheric absorption bands shortward of 3.5 μm which strongly affect the SAAO L filter. These filters are therefore not comparable and photometry of an unsmooth spectrum through these filters will obviously give different results: in particular, Brα affects strongly the ESO L filter and not the SAAO one, while the situation is reversed for the [Ni I] 3.12 μm emission line.

To compare both sets of data, we have used the colour equations from Bouchet et al. (1991d) to transform the SAAO photometry into the ESO system, and we have interpolated the SAAO data to the epochs of our observations by using a polynomial fit to the transformed SAAO light curves. The comparison is illustrated in Fig. 10a–d. These figures show that both sets of J, H and K data are in good agreement, the systematic differences coming from the evolution of the emission lines. However, it is clear that ($L_{ESO} - L_{SAAO}$) monitors the brightening of Brα first, until day ~350, and of [Ni I] 3.12 μm afterwards.

6. The emission lines

The evolution of the spectrum of SN 1987A is by now well known and has been presented and discussed in several places. It is shown in Paper I that the first infrared spectra were described by a strong continuum on which hydrogen emission lines (with P-Cygni profiles) were superimposed. After June 1987, emission lines from other species appeared, and by October the spectra were rich in emission lines arising from ions heavier than hydrogen (whose lines are still, however, the predominant ones). It is clear that medium–high resolution spectra allow a more accurate study of the emission lines than our CVF spectrophotometry (see for instance, Oliva et al. 1987, 1989; Spyromilio et al. 1990; Varani et al. 1990). However, the large time coverage and dense sampling of our data can give interesting clues to the spectroscopic analysis. Therefore, although continuum fitting and blend removal at the low resolution of the CVFs have to be treated with some caution, we have measured the intensities of the stronger lines. The greatest source of uncertainty in these measurements arises from the determination of the continuum.

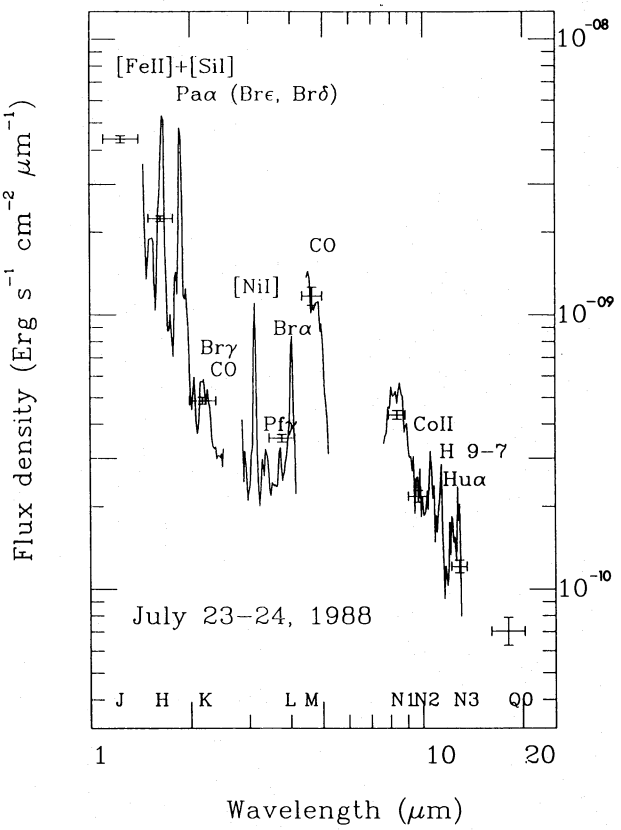

Fig. 8. Broad band photometry and CVF spectra obtained on 23–24 July 1988, and showing the near infrared spectrum of SN 1987A observable from the ground. The identification of the main features is indicated

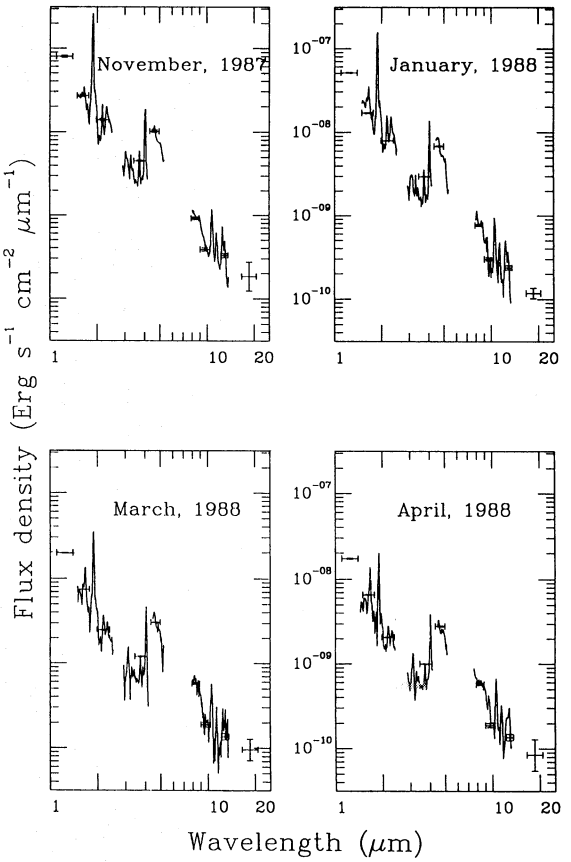

Fig. 9a. Near infrared photometry and CVF spectrophotometry, illustrating the spectral energy distribution of SN 1987A between 1 and 20 μm in November 1987, January 1988, March 1988 and April 1988

6.1. The hydrogen emission lines

The relative intensities of the 12 most measurable lines of hydrogen are consistent with Menzel's case B (Hummer & Storey 1987) at ~30%. We have measured for these lines expansion velocities ranging between 500 and 1400 km s^{-1} with an accuracy better than 200 km s^{-1}: the differences are thus real, and reflect the fact that these lines are not all formed in the same regions of the envelope.

The 3 most prominent lines of hydrogen in the observed spectral range are Paα, Brα and Brγ. The intensity of the Paα line, lying in a strong H_2O atmospheric absorption band, can only be determined in exceptionally good climatic circumstances and, even so, with a low accuracy. The red wing of Brα is placed on the edge of an atmospheric absorption due to CO_2 and H_2O (which defines the photometric *L* window) and then the measurement of this line requires a preliminary fit of its profile. The results relative to Paα, Brα and Brγ are presented in Table 5 and displayed in Fig. 11. All the measurements presented in Table 5 were obtained by integrating the flux density above a continuum level interpolated from shortward of Brγ to the continuum at 3 μm.

The temporal evolution of the intensity of the 3 lines is roughly similar. However, Fig. 11 shows that Paα and Brγ reached their maximum luminosity (between 160 and 200 d after explosion) before Brα (between days 200 and 240). This observation supports the fact that the hydrogen lines are formed in different regions of the envelope, Brα originating in a deeper zone whereas Hα arose from the outermost zone (Danziger et al. 1991a). Then, the intensities decreased monotically at a rate which reproduces the exponential radioactive decay of ^{56}Co. This rate increased around day 300, when the γ-rays started to escape from the envelope. No additional change in the rate of decrease is noticeable at the onset of dust formation, which led to the conclusion that the dust must have been confined to the inner metal-rich parts of the envelope (the ejecta), and did not spread significantly into the hydrogen rich region (Lucy et al. 1991a).

A comparison of Fig. 11 with the one presented in Danziger et al. (1991a) show that the evolution of Paα, Brα and Brγ after maximum is similar to the evolution of Hα. Also, the intensities of the hydrogen lines in the spectrum of SN 1987A vary with time as the intensity of Hα in the

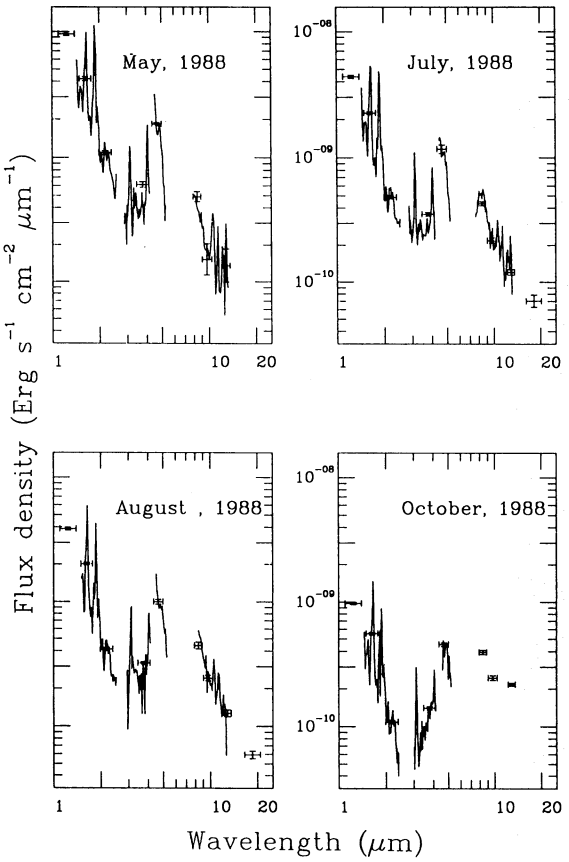

Fig. 9b. Near infrared photometry and CVF spectrophotometry (when available), illustrating the spectral energy distribution of SN 1987A between 1 and 20 μm in May 1988, July 1988, August 1988 and October 1988. Note the sudden growth of the infrared excess between August and October 1988

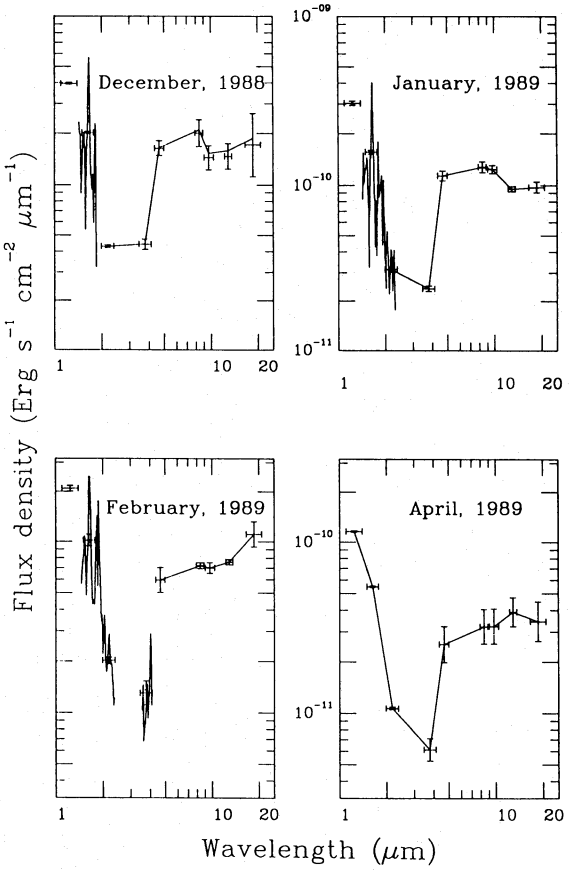

Fig. 9c. Near infrared photometry and CVF spectrophotometry (when available), illustrating the spectral energy distribution of SN 1987A between 1 and 20 μm in December 1988, January 1989, February 1989 and April 1989

type II supernova SN 1980K, measured over a period of 650 d by Uomoto & Kirshner (1986).

6.2. *Other emission lines from stable species*

In the spectral range covered by the CVFs, the line at 1.64 μm is of particular interest. This line has been attributed to a blend of [Fe II] 1.644 μm and [Si I] 1.645 μm (and also to a lesser extent of H 12–4 at 1.641 μm). It has been observed in spectra of supernovae remnants and of the type Ib supernova SN 1983N and the relative contributions of the [Fe II] and [Si I] lines have been discussed by Graham et al. (1986) and Oliva (1987). Modelling and the presence of lines of [Fe II] at other wavelengths suggest that in this blend, the contribution from silicon decreases with time, while that from iron increases. The temporal evolution of the intensity of the blend is shown in Fig. 12. The faster decline observed after day ~530 is related at least in part to the onset of dust formation. The same effect is observed in the evolution of the intensities of [Mg I] 4571 Å and [O I] 6300 Å as discussed in Danziger et al. (1991a) and Lucy et al. (1991a). In these papers, it was argued that the markedly stronger fading of the blend intensity relative to the neighbouring continuum was strongly suggestive of depletion of silicon from the gas phase as a consequence of the formation of silicate grains (which requires a very high condensation efficiency). Lucy et al. (1991a) point out that this data could also be interpreted as a temperature effect, but this would imply a coincidence between the onset of dust formation and an increase in the rate of cooling in the silicon zone, which seems unlikely. Another possibility to explain the difference between line and continuum behaviour is that the continuum is formed in regions less affected by dust. Since silicon is expected to be a minor component of the nuclear composition but a major component of the dust if silicates are formed, efficient condensation into dust might result in this effect (Danziger et al. 1991a).

Figure 13 displays the behaviour of the [Ni I] line at 3.12 μm, as well as the continuum measured at 3.52 and 3.78 μm. It can be seen that the intensity of the [Ni I] line shows, if anything, an even steeper drop in intensity than

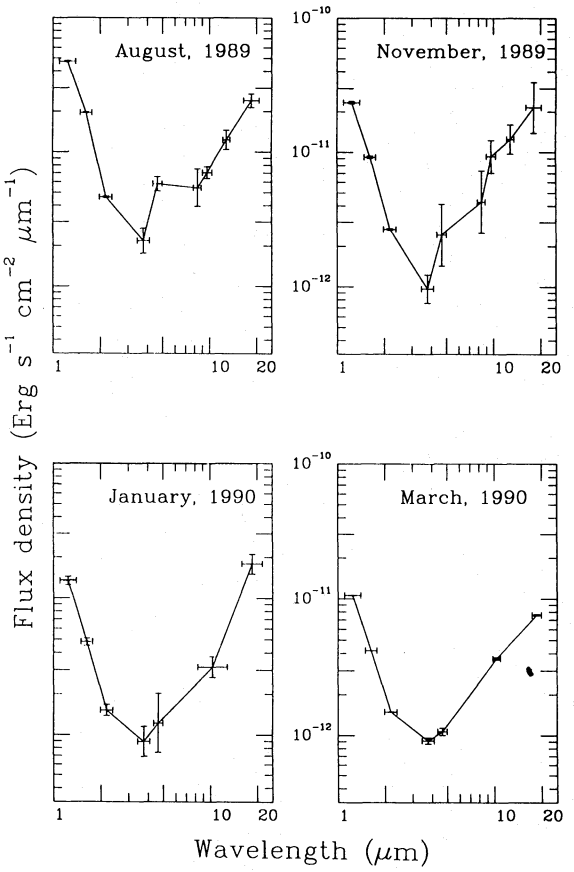

Fig. 9d. Near infrared photometry illustrating the spectral energy distribution of SN 1987A between 1 and 20 μm in August 1989, November 1989, January 1990 and March 1990

that of the [Si I] line. This suggests that either (i) the stable nickel isotopes play a role in dust formation and the evolution of the line intensity can be explained with the same mechanism as the one invoked for silicon, or (ii) other processes may be operating to give rise to the effect observed in the evolution of the intensity of the [O I], [Mg I], [Si I] and [Ni I] lines (as a dramatic extra cooling effect beginning near day 530). We have mentioned above that the 1.644 μm feature is a blend of [Fe II] and [Si I]. Iron would be still increasing in the envelope as a result of radioactive decay of cobalt. Also, the excitation and ionization properties are different for Si I, Fe II and Ni I. For all these reasons modelling is needed to verify which, if either of the above speculative proposals is appropriate.

6.3. *Emission lines from radioactive species*

Before SN 1987A, the evidence for energy input from radioactive decay of ^{56}Co came from light curves and the temporal decay of the Hα luminosity measured in SN 1980K (Uomoto & Kirshner 1986). Our data show even more clearly that the evolution of the bolometric light curve of SN 1987A (Bouchet et al. 1991a; Paper II; Paper III), and of the intensity of some emission lines, as described above, are actually powered by the radioactive decay of ^{56}Co. However, the most convincing evidence for the production of cobalt and its role, as its physical presence in the envelope revealed by emission lines.

In Paper I the presence of a line at 10.52 μm, has been attributed to a transition among fine structure levels in the

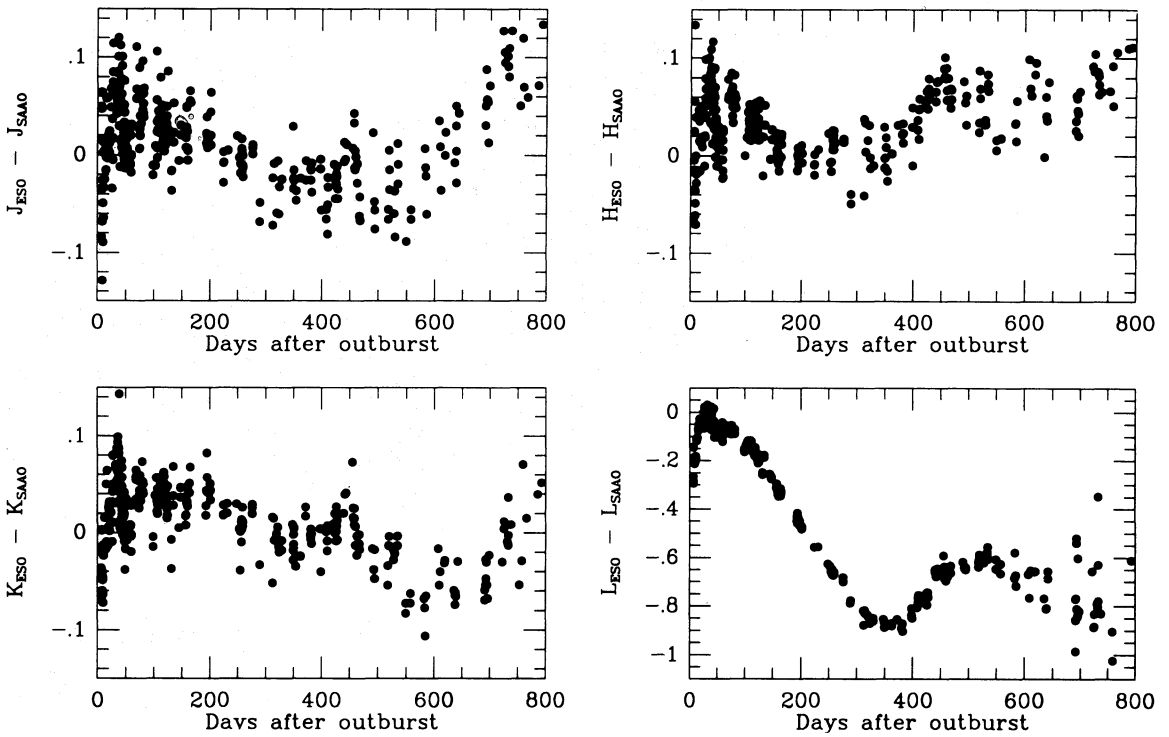

Fig. 10a–d. Comparison between the ESO and the SAAO *J*, *H*, *K*, and *L* photometry, respectively

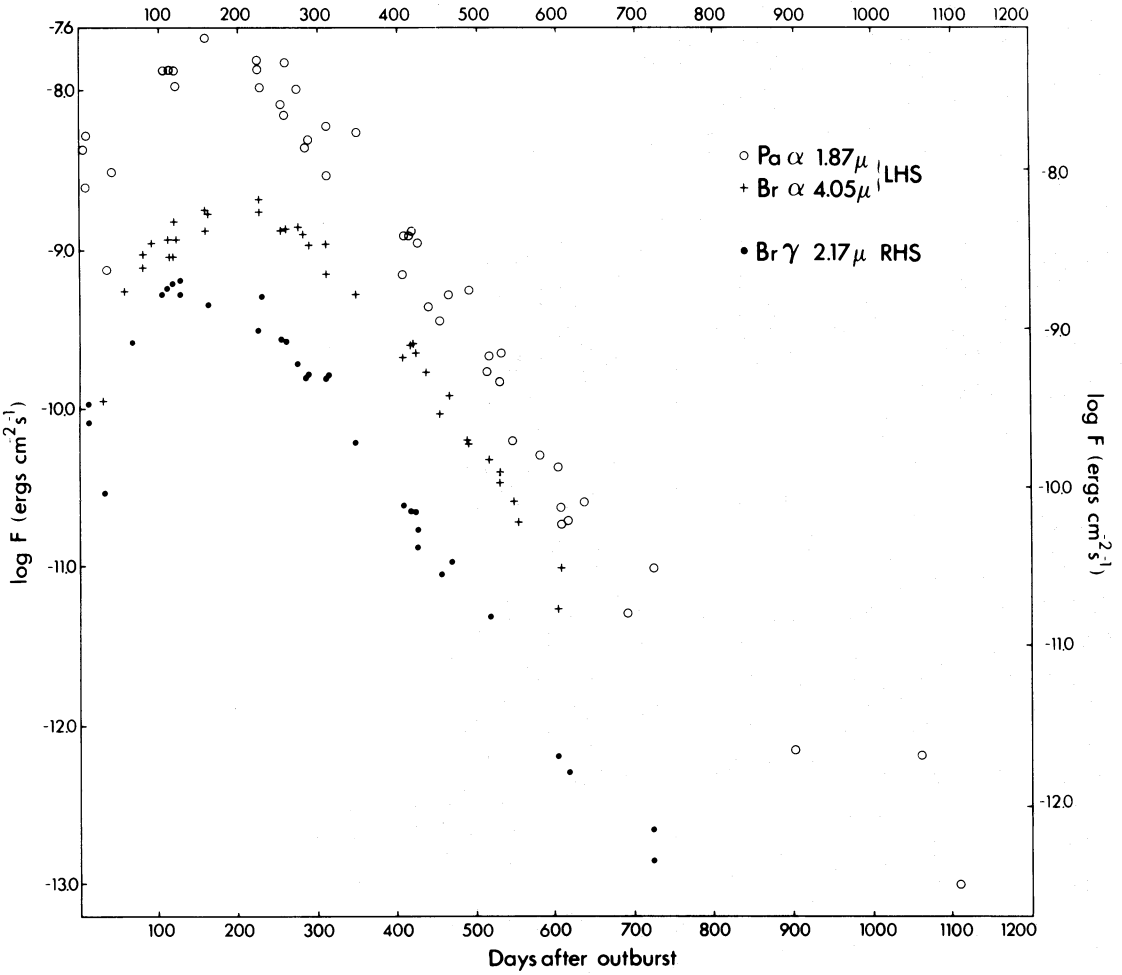

Fig. 11. Temporal evolution of the strengths of the Paα (○), Brγ (●), and Brα (+) hydrogen lines. The flux unit scale is indicated on the left for Brα and Paα, and on the right for Brγ

Table 5a. Analytical representation of the light curves. Magnitude $= A \times t + B$ $t =$ MJD $- 46849.316$

Filter	$125 \leq t \leq 300$ $A \times 10^3$ B	$300 \leq t \leq 535$ $A \times 10^3$ B	$535 \leq t \leq 650$ $A \times 10^3$ B	$650 \leq t \leq 850$ $A \times 10^3$ B	$t \geq 850$ $A \times 10^3$ B
J	12.53(±0.02) 0.561(±0.008)	→ →	19.5(±0.2) −2.98(±0.15)	10.95(±0.2) 2.60(±0.13)	8.36(±0.35) 4.79(±0.35)
H	15.90(±0.07) 0.204(±0.015)	10.66(±0.04) 1.312(±0.017)	19.5(±0.1) −3.45(±0.09)	11.8(±0.2) 1.69(±0.14)	9.4(±0.3) 3.75(±0.25)
K	15.28(±0.02) −0.535(±0.007)	→ →	19.1(±0.1) −2.65(±0.08)	12.6(±0.2) −1.66(±0.15)	6.55(±0.35) 6.71(±0.34)
L	14.08(±0.05) −1.244(±0.011)	11.51(±0.08) −0.496(±0.031)	14.9(±1.5) −2.6(±0.9)	21.(±4.) 6.(±3.)	6.(±1.) 5.5(±1.5)
M	$(215 \leq t) \leftarrow$ $(215 \leq t) \leftarrow$	10.01(±0.05) −1.79(±0.02)	12.(±2.) −2.97(±1.18)	19.(±5.) −7.4(±3.7)	9.(±1.) 0.5(±1.)

Table 5b. Analytical representation of the light curves. Magnitude $= A \times t + B$; $t =$ MJD $- 46849.316$

Filter	$260 \leq t \leq 425$ A $\times 10^3$ B	$600 \leq t \leq 950$ A $\times 10^3$ B
N_1	4.5 (±0.4)	15.6 (±0.5)
	−0.4 (±0.1)	−7.8 (±0.3)
N_2	7.4 (±0.6)	13.3 (±0.6)
	−1. (±0.2)	−6.7 (±0.4)
N_3	7.5 (±0.8)	10.4 (±0.4)
	−2. (±0.25)	−5.9 (±0.3)
Q_0	4.5 (±2.5)	6.9 (±0.5)
	−1.95 (±0.75)	−4.9 (±0.4)

ground state (a^3F) of Co II, which is the predominant ion of cobalt at most phases: the strength of this line is therefore insensitive to temperature. Its temporal behaviour during our monitoring period is shown in Fig. 14. In that plot the points shown for June, 1987 and earlier may not represent detections of the line in question, since the equivalent widths were very small and other lines might have been producing the features present at that time. We note that the peak strength was somewhere in November, 1987 (at day 280 ± 20) and that the strength has been decreasing later. The line vanished between 3 August 1988 (day 526) and 21 November 1988 (day 637) (Bouchet et al. 1991c): this effect is significantly larger than would be expected from radioactive decay alone and has been attributed to extinction by silicate dust in the ejecta (Lucy et al. 1989, 1991a).

The temporal behaviour of the computed mass of cobalt, using always the [Co II] line at 10.52 μm (Danziger et al. 1990, 1991a), has been entirely consistent with theoretical expectation that $\sim 0.075 M_\odot$ of ^{56}Co were formed as part of the nickel–cobalt–iron β-decay. One should note that there are two independent ways of determining the mass of radioactive cobalt, one by measuring the energy input from the radioactive decay and its manifestation in the bolometric light curve (Bouchet et al. 1991a; Paper II; Paper III), and the other by measuring the [Co II] 10.52 μm emission line (Danziger et al. 1990, 1991a). Both methods have associated uncertainties but give similar results. Danziger et al. (1991c) have shown that in the interval day ~400–520, the emission line observations indicate a slightly higher mass. It is just at this epoch that ^{57}Co (with a half-life of 271 d) would begin to contribute

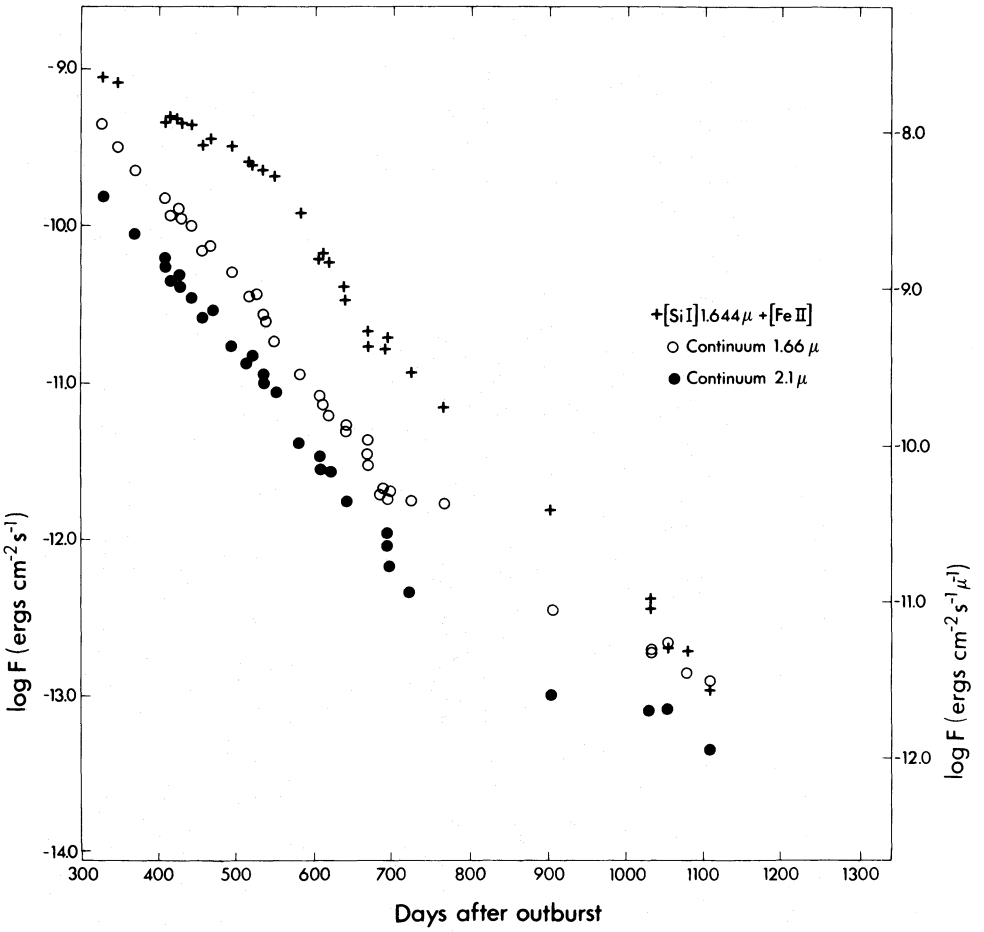

Fig. 12. Temporal evolution of the intensity of the [Si I] + [Fe II] 1.64 μm emission feature (+; left hand scale), and of the flux intensity of the nearby continuum (● = 2.1 μm; ○ = 1.66 μm; right hand scale). The increased rate of decline of the [Si I] line at day ~530 is not so pronounced for the continuum data points. (Reproduced from Danziger et al. 1991a)

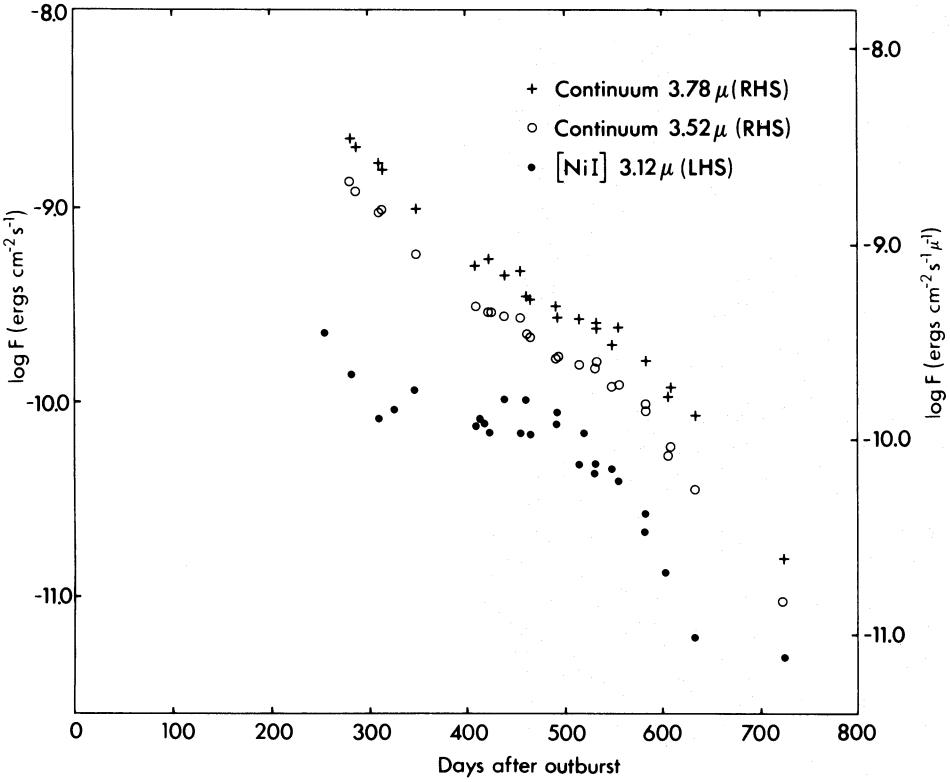

Fig. 13. Temporal evolution of the intensity of the [Ni I] 3.12 μm emission line (●), and of the nearby continuum at 3.52 μm (○) and at 3.78 μm (+). The decrease in the [Ni I] line seems stronger after day ~530 than that for the continuum data points. (Reproduced from Danziger et al. 1991a)

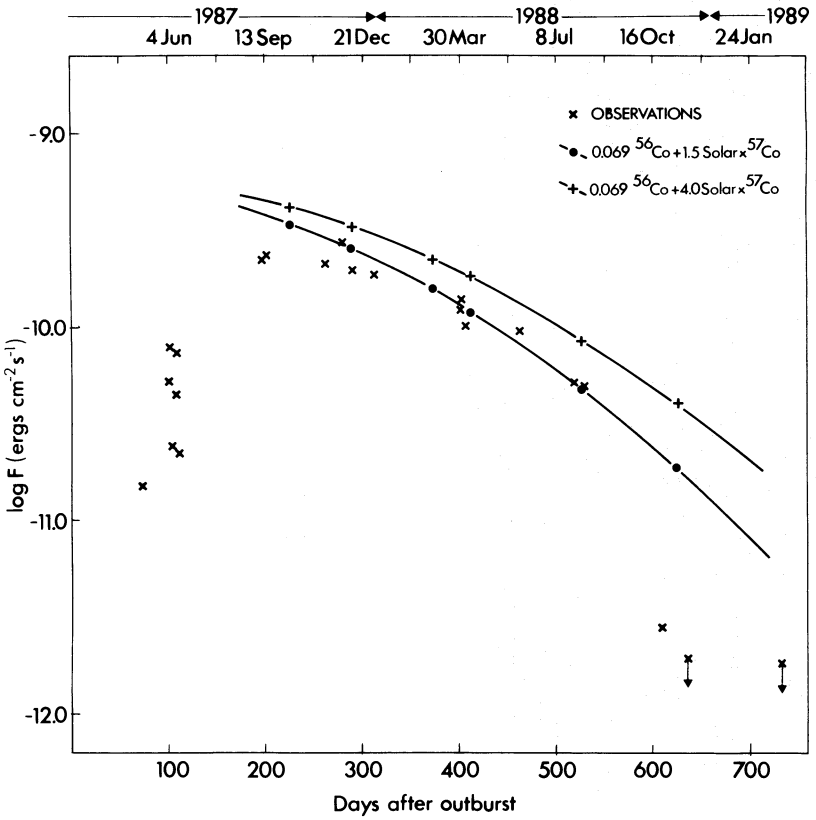

Fig. 14. Temporal evolution of the intensity of the [Co II] 10.52 μm emission line (x) together with the predicted line strengths under the following assumptions: at day 225, Co I/Co I = 1/10, T_e = 4000 K; at day 410, Co I/Co II = 1/2, T_e = 2500 K; at day 525, Co I/Co II = 1/2, T_e = 2000 K; at day 625, Co I/Co II = 2/1, T_e = 2000 K. Note that points plotted near day 100 and earlier should be treated with caution because the intensity measurement of the line was extremely difficult owing to its very small equivalent width

a significant fraction to the line strength if the $^{57}Co/^{56}Co$ production were the same as (or higher than) the ratio of stable isotopes of the same mass found in the solar system (viz. 1/45). Because of the influence of ^{57}Co on the bolometric light curve at late stages (at $t > 1000$) (Paper III; Suntzeff et al. 1991, 1992), it is important to review independent quantitative evidence for the presence of this isotope in the envelope. To determine the amount of radioactive ^{57}Co produced, one can still employ the same methods as for ^{56}Co. However, for its measurable impact on the bolometric luminosity one has to wait longer than for its observable impact on the line strength: this is because the energy released per unit time by ^{57}Co is much lower than by ^{56}Co, as a result of the lower emitted γ-ray energies and the longer half-life of ^{57}Co. A code that synthesizes the emission-line spectrum of a statistically uniform, expanding spheric mass (Danziger et al. 1991a), has been used to calculate the expected line strength of the [Co II] 10.52 μm line assuming that $0.069 M_\odot$ of ^{56}Co was originally produced (Bouchet et al. 1991a), and for different value of the $^{57}Co/^{56}Co$ ratio (viz 1.5 and 4.0 times the amount of ^{57}Co originally suggested by Woosley & Pinto (1988) on the basis of solar system ratios of stable nuclides of 57). Our results (Fig. 14) show unambiguously that during the interval 400–530 d, the observations are best matched with an initial ratio of ~ 1.5 solar. They also show that at day 520 the mass of the two isotopes of cobalt would be equal at $0.0007 M_\odot$, and that later than this ^{57}Co would dominate in mass (Danziger et al. 1990, 1991c).

Two other [Co II] lines are located in the spectral range covered by the CVFs. One, at 1.634 μm lies in the blue wing of the [Fe II] + [Si I] blend at 1.64 μm and cannot be detected. The other one at 1.547 μm has been observed by Varani et al. (1990): it is blended with [Fe II] 1.533 μm and [Fe I] 1.535 μm and to study it requires a higher spectral resolution than that provided by the CVFs. Our result that the $^{57}Co/^{56}Co$ is 1.5 the solar system ratio is in good agreement with the analysis of the [Co II] 1.547 μm line by Varani et al. (1990), and with the upper limit from the X-ray emission following the Comptonized γ-ray lines from the ^{57}Co decay reported by Sunyaev et al. (1990). Although there are uncertainties with these observationally derived ratios, associated with the observations and with the mass determination (viz. oscillator strengths, estimates of the relevant proportions of the different ionization stages and to a lesser extent the temperature), our results do impose constraints. In particular, we note that our observations suggest that the $^{57}Co/^{56}Co$ ratio might even be less than 1.5 if our estimate of the correction for the proportion of Co I is too high (Danziger et al. 1991c): other published estimates of the Co I/Co II ratio indicate that to date our estimate of this

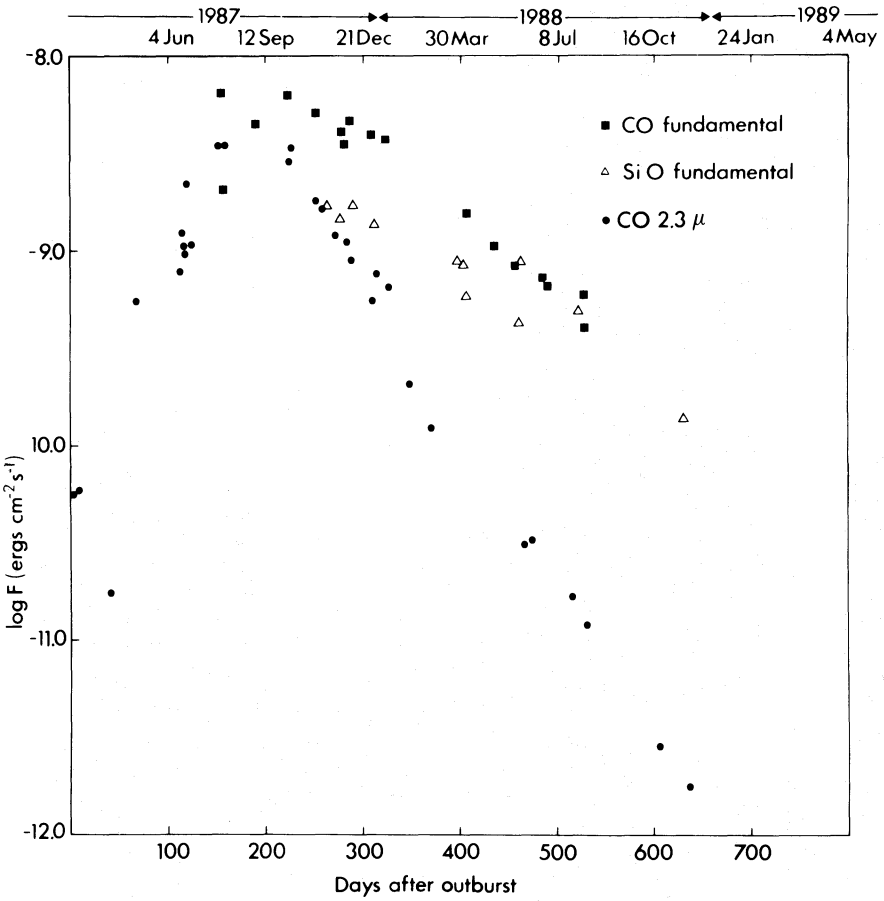

Fig. 15. Temporal evolution of the flux in the CO 2.3 μm first overtone band, and in the CO 4.6 μm (●) and SiO 8 μm (Δ) fundamental bands

ratio is the highest. Therefore, we believe that the uncertainties in our determination are not large enough to encompass the possibility that $^{57}Co/^{56}Co$ is as high as 4, a value quoted by Suntzeff et al. (1991, 1992) to explain the flattening of the late-time bolometric luminosity. Our results seems to be nicely confirmed by the recent observations of γ-rays from the decay of ^{57}Co with the Oriented Scintillation Spectrometer on the Compton Gamma Ray Observatory announced by Kurfess et al. (1992).

Thus, either an additional energy input is needed to fit the late time bolometric light curve (as discussed in Paper III), or some of the fundamental assumptions used in the modelling are in error.

In that respect, it is very unfortunate that the occurence of dust and the cooling of the envelope have prevented this more direct determination of the $^{57}Co/^{56}Co$ ratio at later epochs.

6.4. *The CO and SiO emissions*

As shown in Danziger et al. (1991a), the only authentically identified molecular species in the envelope of SN 1987A are carbon monoxide (CO) and silicon monoxide (SiO). There is however a recent claim for the identification of H_3^+ in the 3 μm region of the spectrum by Miller et al. (1992). Two vibration–rotation bands of CO are located in the spectral range covered by the CVFs: the fundamental at 4.6 μm and the first overtone at 2.3 μm. The fundamental vibration–rotation band of SiO is apparent near 8 μm: since the shorter wavelength half of this band is not transmitted through the atmosphere we see only the long wavelength side of it. Our results show that during the interval 150–500 d the CO fundamental band strength is always a factor 2–3 greater than the SiO fundamental band strength.

The CO molecule was first detected at La Silla in June 1987 (Paper I; Danziger et al. 1988). The slope of the continuum was determined as in Paper I. Figure 15 shows the temporal dependence of the flux in the first overtone band (2.3 μm) of CO, and in the fundamental bands of CO and SiO. Because of the temporal variation of temperature, density, optical depth and CO formation, the behaviour of the light curves displayed in Fig. 15 has to be interpreted through modelling. Nevertheless, Fig. 15 shows that CO had a peak strength at day 152 and at day 370 was emitting at 3% of the peak flux. The intensities of the CO and SiO band emissions are given in Tables 6–8.

Our observations of band strengths show that after day ~200 the fundamental and first overtone band strengths decrease at different rates. It has been shown in Paper I and in Danziger et al. (1988) that the analysis of the slopes of the bandhead emissions (Young 1968) shows that the temperature decreases from $T=4000\pm500$ K at days 105–120 (mid-June 1987), to $T=2000\pm500$ K at day 230 (October 12, 1987). This result is confirmed by data obtained at La Silla by Oliva et al. (1987) at a higher

Table 6. Intensities of hydrogen lines (log erg s^{-1} cm^{-2})

Date	Day	Paα	Brα	Brγ
28/02/87	4	−8.37		
04/03/87	8	−8.61		−9.49
05/03/87	9	−8.29		−9.61
30/03/87	34	−9.13	−9.95	−10.05
06/04/87	41	−8.52		
23/04/87	58		−9.28	
01/05/87	66	−7.63		−9.10
14/05/87	79		−9.03	
15/05/87	80		−9.12	
05/06/87	102			−8.79
10/06/87	107	−7.88		−8.76
13/06/87	110		−8.96	
15/06/87	112	−7.86		−8.72
16/06/87	113		−8.95	
19/06/87	116		−9.05	
20/06/87	117		−9.05	
23/06/87	120		−8.82	
24/06/87	121	−7.87	−8.93	−8.71
25/06/87	122	−7.97		−8.80
31/07/87	158	−7.67	−8.87	−8.85
02/08/87	159		−8.77	
05/08/87	162		−8.77	
05/09/87	193	−7.80		−8.75
09/09/87	197	−7.98		−8.80
05/10/87	223		−8.76	
06/10/87	225	−7.85	−8.68	−9.01
04/11/87	253	−8.08		−9.07
05/11/87	254		−8.87	
07/11/87	256		−8.87	
08/11/87	257	−8.16		
09/11/87	258	−7.82		−9.09
25/11/87	274	−7.99	−8.85	−9.23
03/12/87	282		−8.90	
04/12/87	283	−8.36		−9.31
08/12/87	287	−8.30	−8.97	−9.29
31/12/87	310	−8.53	−8.95	−9.32
03/01/88	313	−8.21	−9.15	−9.32
07/02/88	348	−8.26		−9.73
08/02/88	349		−9.28	
29/02/88	370	−7.76		−8.79
07/04/88	408	−8.92		−10.16
08/04/88	409	−9.15	−9.67	−10.13
14/04/88	415	−8.92	−9.59	−10.15
19/04/88	420	−8.90		−10.16
21/04/88	422		−9.65	
23/04/88	424			−10.38
24/04/88	425	−8.96		−10.27
07/05/88	438		−9.76	
09/05/88	440	−9.37		
23/05/88	454	−9.45	−10.03	−10.56
03/06/88	465		−9.92	
04/06/88	466	−9.29		−10.48
28/06/88	490		−10.19	
30/06/88	492	−9.25		−10.21
23/07/88	515	−9.78		−10.33
25/07/88	517	−9.68		−10.82
08/08/88	531	−9.65		−10.39

Table 6 (continued)

Date	Day	Paα	Brα	Brγ
09/08/88	532	−9.83	−10.45	
24/08/88	547	−10.21	−10.59	
01/09/88	555		−10.72	
27/09/88	581	−10.30		
19/10/88	603	−10.38	−11.28	−11.70
22/10/88	606	−10.63		
23/10/88	607		−11.02	
25/10/88	609	−10.74		
02/11/88	617	−10.72		−11.79
22/11/88	637	−10.60		
14/01/89	690	−11.30		
16/02/89	723	−11.01		−12.15
15/08/89	903	−12.16		
11/01/90	1052	−12.19		
09/03/90	1109	−13.00		−13.71

Table 7. Intensities of the first overtone CO band (log erg^{-1} cm^{-2})

Date	Day	CO 2.3 μm
04/03/87	8	−10.22
05/03/87	9	−10.25
06/04/87	41	−10.75
01/05/87	66	−9.25
15/06/87	112	−9.11
18/06/87	115	−9.08
20/06/87	117	−9.05
21/06/87	118	−8.96
24/06/87	121	−8.65
25/06/87	122	−8.97
30/07/87	157	−8.53
01/08/87	158	−8.45
05/09/87	224	−8.54
09/09/87	228	−8.55
14/11/87	253	−8.83
09/11/87	258	−8.85
25/11/87	274	−9.00
04/12/87	283	−8.96
08/12/87	287	−9.13
31/12/87	310	−9.37
03/01/88	313	−9.18
17/01/88	327	−9.19
07/02/88	348	−9.68
29/02/88	370	−9.91
23/05/88	454	−10.48
04/06/88	466	−10.50
25/07/88	517	−10.77
08/08/88	531	−10.91
22/10/88	606	−11.54
22/11/88	637	−11.75

spectral resolution. In the optically thin case, the intensity ratio between the fundamental and the first overtone CO bands for temperatures near 2000 K is ~20 (Young 1968). Our results give a ratio of ~1.5 (within the uncertainties)

Table 8. Intensities of the fundamental CO band (log erg s^{-1} cm^{-2})

Date	Day	CO 4.6 μm
30/07/87	157	−8.21
02/08/87	159	−8.70
04/09/87	192	−8.35
05/10/87	223	−8.21
05/11/87	254	−8.30
03/12/87	282	−8.40
08/12/87	287	−8.36
03/01/88	313	−8.42
17/01/88	327	−8.44
08/04/88	409	−8.86
07/05/88	438	−8.98
25/05/88	456	−8.95
30/05/88	461	−9.08
28/06/88	490	−9.15
30/06/88	492	−9.17
08/08/88	531	−9.24
09/08/88	532	−9.38

Note: Integrated 4.5–5.2 μm then × 1.16 for unseen part of band.

Table 9. Intensities of the fundamental SiO band (log erg s^{-1} cm^{-2})

Date	Day	SiO
12/11/87	261	−8.79
29/11/87	278	−8.84
10/12/87	289	−8.78
02/01/88	312	−8.87
02/04/88	403	−9.07
06/04/88	407	−9.24
31/05/88	462	−9.07
01/06/88	463	−9.37
03/04/88	526	−9.30
21/11/88	637	−9.84

Note: Integrated 8.2–9.6 μm then × 2 to correct for unseen part.

at day 200. A much lower ratio than expected is also reported by Oliva et al. (1987) who interpreted this as self absorption of the fundamental band. The ratio of the strengths of the fundamental to the first overtone CO bands has increased dramatically with time to reach a value of ~32 at day ~500, indicating that the decrease in absolute strength of the fundamental band has been much slower than that of the first overtone band: whether there has been a fundamental change in the actual mass of CO while the strength of the first overtone has decreased by a factor 200 remains to be modelled (Danziger et al. 1991a). The most recent estimate of the mass of CO is that by Lin et al. (1992) who obtain $10^{-3} M_{\odot}$ constant from day 192 to day 377.

Oliva et al. (1987) determined an expansion velocity of 1000 km s^{-1} at days 224–227 (5–8 October 1987), similar to (although sightly higher than) the measured velocities of the atomic lines, which indicates that the CO emission arises from the same regions of the ejecta as do the other species.

7. Conclusions

The monitoring of SN 1987A undertaken at ESO has led to several major findings. In this paper, we report on the infrared observations obtained until March 1991, on which these works have been based.

1. These data include the broad band photometric light curves (from J to Q_0) and the temporal evolution of the spectral energy distribution.

2. We compare our photometric results with those of SAAO.

3. We present the evolution with time of the intensities of the most prominent emission features – hydrogen, [Fe II], [Si I], [Ni I], [Co II], CO and SiO – and discuss qualitatively some problems associated with our observations. In particular, our results exclude the possibility that the initial $^{57}Co/^{56}Co$ ratio was as high as 4 times that indicated by solar system isotope ratios.

4. Our infrared photometry shows that dust is still present at least until day ~1400. This result is consistent with independent contemporaneous high-resolution spectral analysis which shows that emission lines are still blue-shifted (Danziger et al. 1991b, c).

5. A somewhat simplistic two-zone model for the envelope has been proposed by Danziger et al. (1991b, c) to account for visible spectroscopic observations: one hotter region with higher velocity and another cooler with lower velocity. We show that this model accounts also for the observed changes in the near-IR colours in the period starting from day ~530 (onset of dust formation) through day ~650 (end of the bulk of dust formation), until day ~760 (emergence of the hotter material).

The infrared photometry reported here is quite consistent with, and supports results from visible spectroscopy. This demonstrates – yet again – that whatever the physical processes involved, both types of observations are interrelated. The example of SN 1987A therefore reinforces the importance of obtaining closely spaced and contemporaneous observations at all wavelengths, and especially from the ground, optical and infrared data.

Acknowledgements. The work presented in this paper is part of a more general effort undertaken at ESO for the study of SN 1987A. In particular, we want to acknowledge the fruitful collaboration with Drs. L.B. Lucy and C. Gouiffes. We are especially grateful to Mrs. R. Vega and E. Matamoros, because their constant and enthusiastic support – both observational and technical – during all these observations have been fundamental for the success of this monitoring. Many thanks are also due to the electronic staff of the infrared team at La Silla: Mrs. J. Roucher, H. Gamperlein and U. Weilenmann. The support of the former Directors General of ESO, Prof. L. Woltjer, and Prof. van der Laan, and of the O.P.C., have been fundamental to the accumulation of this data at ESO, La Silla.

References

Bersanelli M., Bouchet P., Falomo R., 1991, A&A 252, 854
Bouchet P., 1989, The infrared Photometers, ESO Operating Manual No. 11
Bouchet P., 1990, Thèse de l'Université de Paris VII, November 1990
Bouchet P., Stanga R., Le Bertre T., Epchtein N., Hamann W.R., Lorenzetti D., 1987, A&A 177, L9
Bouchet P., Moneti A., Slezak E., Le Bertre T., Manfroid J., 1989a, A&AS 80, 379 (Paper I)
Bouchet P., Danziger I.J., Lucy L.B., 1989b, IAU Circ. No. 4933
Bouchet P., Phillips M.M., Suntzeff N.B., Gouiffes C., Hanuschik R.W., Wooden D.H., 1991a, A&A 245, 490
Bouchet P., Danziger I.J., Lucy L.B., 1991b, AJ 99, 650 (Paper III)
Bouchet P., Danziger I.J., Lucy L.B., 1991c, in: Woosley S. (ed.) Supernovae, Proc. Tenth Santa-Cruz Summer Workshop in Astronomy and Astrophysics. Santa Cruz, July 10–21, 1989. Springer, New York, p. 49
Bouchet P., Manfroid J., Schmider F.-X., 1991d, A&AS 91, 409
Carter B.S., 1990, MNRAS 242, 1
Catchpole R.M., et al., 1987, MNRAS 229, 15p
Catchpole R.M., et al., 1988, MNRAS 231, 75p
Catchpole R.M., et al., 1989, MNRAS 237, 55p
Danziger I.J., Bouchet P., Fosbury R.A.E., Gouiffes C., Lucy L.B., Moorwood A.F.M., Oliva E., Rufener F., 1988, in: Kafatos M., Michalitsianos A. (eds.) The Fourth George Mason Fall Workshop in Astrophysics: SN 1987A in the LMC. October 1987, George Mason University, Fairfax, U.S.A., Cambridge University Press, Cambridge, p. 37
Danziger I.J., Bouchet P., Gouiffes C., Lucy L.B., 1989, IAU Circ. No. 4746
Danziger I.J., Bouchet P., Gouiffes C., Lucy L.B., 1990, in: Ferrini F., Franco J., Matteucci F. (eds.) Proc. of The Elba EIPC Workshop on Chemical and Dynamical Evolution of Galaxies, Marciana Marina, Isola d'Elba, Italy, September 4–14, 1989. PISA, ETS Editrice, p. 340
Danziger I.J., Lucy L.B., Bouchet P., Gouiffes C., 1991a, in: Woosley S (ed.) Supernovae, Proc. Tenth Santa-Cruz Summer Workshop in Astronomy and Astrophysics, UC Santa Cruz, July 10–21, 1989. Springer, New York, p. 69
Danziger I.J., Bouchet P., Gouiffes C., Lucy L.B., 1991b, in: Danziger I.J., Kjär K. (eds.) Proc. ESO/EIPC Workshop on SN 1987A and other Supernovae. Marciana Marina, Isola d'Elba, Italy, September 17–22, 1990, p. 217
Danziger I.J., Bouchet P., Gouiffes C., Lucy L.B., 1991c, ESO/CERN/TEXAS workshop on Relativistic Astrophysics, December 1990, New York Academy of Science (in press)
Glass I.S., 1985, Ir. Astron. J. 17, 1
Graham J.R., Meikle W.P.S., Allen D.A., Longmore A.J., Williams P.M., 1986, MNRAS 218, 93
Hummer D.G., Storey P.J., 1987, MNRAS 224, 801
Kurfess et al., 1992, AJ 399, L137

Lin, Dalgarno A., Lepp S., 1992, AJ (in press)
Lucy L.B., 1991, in: Danziger I.J., Kjär K. (eds.) Proc. ESO/EIPC Workshop on SN 1987A and other Supernovae. Marciana Marina, Isola d'Elba, Italy, September 17–22, 1990, p. 457
Lucy L.B., Danziger I.J., Gouiffes C., Bouchet P., 1989, in: Tenorio-Tagle G., Moles M., Melnick J. (eds.) Structure and dynamics of Interstellar Medium, Lecture Notes in Physics. Springer, Berlin, Vol. 350, p. 164
Lucy L.B., Danziger I.J., Gouiffes C., Bouchet P., 1991a, in: Woosley S. (ed.) Supernovae, Proc. Tenth Santa-Cruz Summer Workshop in Astronomy and Astrophysics, UC Santa Cruz, July 10–21, 1989. Springer, New York, p. 82
Lucy L.B., Danziger I.J., Gouiffes C., 1991b, A&A 243, 223
Miller S., Tennyson J., Lepp S., Dalgarno A., 1992, Nat 355, 420
Meikle W.P.S., Allen D.A., Spyromilio J., Varani G.-F., 1989, MNRAS 238, 193
Menzies J.W., et al., 1987, MNRAS 227, 39p
Oliva E., 1987, AJ 321, L45
Oliva E., Moorwood A.F.M., Danziger I.J., 1987, Messenger 50, 18
Oliva E., Moorwood A.F.M., Danziger I.J., 1989, in: Proc. 22nd ESLAB Symposium on Infrared Spectroscopy in Astronomy, Salamanca (Spain), December 1988, ESA SP-290, p. 375
Rank D.M., Pinto P.A., Woosley S.E., Bregman J.D., Witteborn F.C., Axelrod T. S., Cohen M., 1988, Nat 331, 505
Spyromilio J., Meikle W.P.S., Allen D.A., 1990, MNRAS 242, 669
Spyromilio J., Stathakis R.A., Cannon R.D., 1991, in: Danziger I.J., Kjär K. (eds.) The ESO/EIPC Workshop: SN 1987A and other Supernovae. Marciana Marina, Isola d'Elba, 17–22 September 1990, p. 225
Suntzeff N.B., Bouchet P., 1990, AJ 99, 650 (Paper II)
Suntzeff N.B., Phillips M.M., Elias J.H., Depoy D., Walker A.R., 1991, AJ 102, 1118
Suntzeff N.B., Phillips M.M., Elias J.H., Depoy D., Walker A.R., 1992, ApJ 384, L33
Sunyaev A.E., et al., 1990, Sov. Astron. Lett. 16, 403
Uomoto A., Kirshner R.P., 1986, ApJ 308, 685
Varani G.-F., Meikle W.P.S., Spyromilio J., Allen D.A., 1990, MNRAS 245, 570
West R.M., Lauberts A., Jorgensen H.E., Schuster H.-E., 1987, A&A 177, L1
Whitelock P.A., et al., 1988, MNRAS 234, 5p
Whitelock P.A., et al., 1989, MNRAS 240, 7p
Wooden D.H., 1990, Ph.D. Thesis, University of California, Santa Cruz, 1989
Woosley S.E., Pinto P.A., 1988, in: Gehrels N., Share G. (eds.) Nuclear Spectroscopy of Astrophysical Sources, AIP Conf. Proc. 170. AIP, New York, p. 87
Young L.A., 1968, J. Quant. Spectrosc. Radiat. Transfer 8, 693